THE JOURNAL OF FINANCE • VOL. LXXIV, NO. 1 • FEBRUARY 2019

How Crashes Develop: Intradaily Volatility and Crash Evolution

DAVID S. BATES*

ABSTRACT

This paper explores whether affine models with volatility jumps estimated on intradaily S&P 500 futures data over 1983 to 2008 can capture major daily outliers such as the 1987 stock market crash. Intradaily jumps in futures prices are typically small; self-exciting but short-lived volatility spikes capture intradaily and daily returns better. Multifactor models of the evolution of diffusive variance and jump intensities improve fits substantially, including out-of-sample over 2009 to 2016. The models capture reasonably well the conditional distributions of daily returns and realized variance outliers, but underpredict realized variance inliers. I also examine option pricing implications.

WHAT IS A CRASH? IN THE jump-diffusion model of Merton (1976), a crash is a rare event—a single adverse draw from a Poisson counter, with a vanishingly small probability of multiple adverse draws within a single day. While this model may be successful at capturing outliers in daily returns, it does not appear to capture the intradaily evolution of major market downturns. The 28% drop in the December 1987 S&P 500 futures price (23% drop in the S&P index) on Monday, October 19, 1987, from the preceding Friday's closing level did not occur within five minutes, for instance; it took all day to achieve the full decline. Indeed, papers such as Tauchen and Zhou (2011) that use the bipower variation approach of Barndorff-Nielsen and Shephard (2004, 2006) to decompose realized variance into diffusive and jump components suggest there were no jumps at all on October 19. Instead, it was a draw of roughly two standard deviations on a day that happened to have an unusually high intradaily realized volatility of 12%.

While the increasing availability of high-frequency data has led to exploration of intradaily volatility evolution, including in stock markets, there has been little direct estimation of dynamic models with stochastic volatility and

*David Bates is with the University of Iowa and the National Bureau of Economic Research. I am grateful for comments on earlier versions of the paper from seminar participants at Iowa, Northwestern, Houston, Lugano, and the Collegio Carlo Alberto and from conference participants at the 2012 IFSID Conference on Structured Products and Derivatives, McGill University's 2014 Risk Management Conference, the 2016 FMA/CBOE Conference on Volatility and Derivatives, and the 2017 annual conferences of the Midwest Finance Association and Society for Financial Econometrics. I have read the *Journal of Finance*'s disclosure policy and have no conflicts of interest to disclose.

DOI: 10.1111/jofi.12732

jumps using intradaily data. Papers such as Andersen and Bollerslev (1997) focus on volatility dynamics; in particular, on reconciling GARCH-based volatility evolution estimates from daily versus intradaily data. As described by Andersen (2004), the recognition that realized variance effectively summarizes intradaily volatility information *and* sidesteps the challenges in fitting pronounced diurnal volatility patterns and announcement effects has led intradaily research to shift focus to realized variance. Whether jumps are important has been assessed indirectly in this literature, with either the bipower variation approach of Barndorff-Nielsen and Shephard (2004, 2006) or the threshold approach of Mancini (2009) used to assess intradaily jump contributions to realized variance. These approaches maintain the Merton (1976) presumption that jumps are rare.

This indirect evidence and more direct parametric estimates by Stroud and Johannes (2014) on intradaily data point to a fundamental mismatch between jump magnitudes from intradaily versus from daily stock market data, let alone those inferred from option prices. Stroud and Johannes (2014) find that the standard deviation of unexpected jumps in five-minute returns is between 0.2% and 0.4%, and that magnitudes for predictable announcement effects are similar. The jump magnitudes estimated by Bates (2012, Table VI) on daily data over the 1926 to 2006 period using a double exponential jump distribution are an order of magnitude higher: −2.1% on average for negative jumps and +1.6% for positive jumps. The double exponential jump parameters inferred from stock index options by Andersen, Fusari, and Todorov (2015) are even larger: −3.9% on average for risk-neutral negative jumps and +2.7% for risk-neutral positive jumps. Of course, one must be wary of parameter inferences from option prices, as standard equity and volatility risk premia imply that the frequency and magnitude of negative jumps are greater under the risk-neutral than under the actual distribution. However, those effects are reversed for positive jumps, implying that one should observe even larger (and more frequent) positive jumps on average than the +2.7% estimate in Andersen, Fusari, and Todorov (2015).

The objective of this paper is to bridge the gap between intradaily and daily evidence on stock market returns and to explore continuous-time affine models that might be compatible with both. The key feature of the models is "self-exciting" synchronous and correlated jumps in intradaily stock returns and volatility, which is essentially a stochastic-intensity version of the Duffie, Pan, and Singleton (2000) constant-intensity volatility jump model. Every small intradaily jump substantially increases the probability of more intradaily co-jumps in volatility and returns, and these multiple price jumps can accumulate into the major outliers in daily returns that we occasionally observe. The model is estimated on intradaily and overnight S&P 500 futures returns over the 1983 to 2008 period using Bates's (2006, 2012) approximate maximum likelihood (AML) filtration methodology, taking into account special features of intradaily futures data. Estimates are then tested for compatibility with daily returns—including movements exceeding 10% in 1987 and 2008. The 2009 to 2016 period is used for out-of-sample tests of the model.

The two central mechanisms of the model are volatility feedback (via jumps) and leverage; that is, a tendency of conditional volatility to become more volatile at higher levels combined with negative correlations between price and volatility shocks. These mechanisms have previously been proposed and estimated on daily data using a variety of models and estimation methodologies. The diffusive affine stochastic volatility model of Heston (1993) has both, and is estimated on daily stock market data by various authors surveyed in Bates (2006, Table 7). The nonaffine diffusive log variance models in Chernov et al. (2003) have substantial volatility feedback; the diffusive power variance model in Jones (2003) has even more. Models with jumps typically have leverage but not volatility feedback through jump channels, for example, the price/volatility cojump model of Eraker, Johannes, and Polson (2003) estimated on daily data and the cojump model of Stroud and Johannes (2014) estimated on intradaily data. Both of these papers use the Monte Carlo Markov chain estimation methodology and have constant-intensity rather than self-exciting jumps. Calvet and Fisher (2008) propose a tightly parameterized Markov chain model for daily log variance evolution that also lacks volatility feedback. Aït-Sahalia, Cacho-Diaz, and Laeven (2015) and Fulop, Li, and Wu (2015) employ affine models with stochastic volatility and self-exciting volatility jumps, which they estimate on daily stock market data. Andersen, Fusari, and Todorov (2015) have a model of self-exciting price/volatility cojumps similar to this paper's model, but their estimation methodology differs in relying heavily on matching options data.

The nonparametric literature, of course, makes extensive use of intradaily returns, typically at a five-minute horizon. That literature focuses primarily on decomposing intradaily realized variance into diffusive and jump components, and on developing tests of the null hypothesis of no jumps or cojumps.[1] Such analyses can also be conducted in the affine parametric framework used here. Indeed, as discussed below, any affine latent characteristic can be estimated from observed data using Bayesian filtration methods: the number and size of stock market jumps, quadratic variation and its diffusive variance and squared jump components, and even the magnitude of volatility jumps. Nested models without volatility jumps can be tested via standard likelihood ratio tests.

The key difference between this paper and prior realized variance papers is its focus on the intradaily *dynamics* of diffusive variance and jump intensities. Nonparametric estimates have an aliasing problem: if integrated diffusive variances are estimated each day from intradaily data by bipower variation or threshold techniques, the approach can at best describe the daily dynamics of the series. This paper, by contrast, estimates dynamic models on intradaily data to see whether volatility feedback in the form of self-exciting volatility/price cojumps is present at intradaily frequencies. The sign and magnitude of every 15-minute return contains important information for the probability of future

[1] See Jacod and Todorov (2010) for statistical tests of price/volatility cojump models, and Bandi and Renò (2016) for nonparametric estimates of cojump models on S&P futures returns over the 1982 to 2009 period. The latter includes a model in which the mean and volatility of price jumps are affected by the level of conditional volatility—another form of volatility feedback.

price/volatility cojumps over the next 15 minutes. This information includes not just the large price movements that nonparametric methods can readily identify as jumps, but also the more ambiguous returns of three to five diffusive standard deviations that *might* be jumps.[2] The explicit parametric models in this paper provide the structure for extracting that information via a recursive filtration procedure that updates assessments of the underlying diffusive volatility and jump intensity state variables every 15 minutes.

I address four issues. First is the issue of identifying the appropriate time-series model. To that end, I use an extensive history of intradaily and overnight S&P 500 futures returns over the 1983 to 2008 period that includes the extreme stock market movements in October 1987 and in the fall of 2008. Moreover, I build up the models progressively. I start with a model that has price jumps but not volatility jumps. I then add volatility cojumps, and finally add richer dynamics for the evolution of diffusive volatility and jump intensities. I also look at models without the self-exciting feature. I find that multifactor models with self-exciting but short-lived volatility spikes substantially improve model fits both in-sample and out-of-sample.

Second is the issue of time aggregation; that is, whether various proposed affine models estimated using 15-minute returns actually capture the statistical properties of daily returns, including the major daily outliers in 1987 and 2008. Affine models are especially well suited for exploring this issue, because affine models time-aggregate. An affine model for intradaily returns implies an affine model for daily returns that can be used for standard QQ diagnostics of conditional distributions.

Third is the issue of how well the models capture the statistical properties of daily realized variances. Insofar as realized variance is approximately quadratic variation, which is affine, QQ diagnostics similar to those used for daily returns can be used for realized variances. (In practice, simulation-based bias corrections prove necessary.) I also look at how well various models forecast realized variances at 1- to 21-day horizons, as a precursor to the final model criterion: how well the models fit short-maturity option prices.

The paper is organized as follows. Section I describes the intradaily and overnight data, the multifactor models and estimation methodology, and how well the models fit. Section II contains additional diagnostics using intradaily realized variance, while Section III explores option pricing fits. Section IV concludes. Overall, the multifactor affine models with volatility spikes do a reasonably good job of matching the properties of intradaily and daily S&P 500 futures returns, especially as more factors are added. Furthermore, the most general three-factor model captures the occasionally extreme observations of realized variance reasonably well—which is when extreme daily stock market returns occur. The models underpredict the frequency of small realized variance observations, however, which indicates that some specification error remains. Similarly, the more general models fit the overall level of options' implicit

[2] See Bates (2006, pp. 942–943) or Aït-Sahalia and Jacod (2014, pp. 118–119) for discussions of this issue.

volatilities progressively better, but all models have difficulty matching the slope of the volatility smirk at maturities greater than the shortest one-day horizon considered.

I. Data and Models

A. Data

S&P 500 futures began trading at the Chicago Mercantile Exchange (CME) on April 21, 1982, using the open-outcry pit trading prevailing at the CME at that time for all futures contracts. Initial trading hours were 9 AM to 3:15 PM Central Standard Time, with CME pit trading typically extending 15 minutes beyond trading at the New York Stock Exchange (NYSE).[3] On September 30, 1985, the NYSE and CME shifted the opening time to 8:30 AM CST. Starting in December 1990, both the NYSE and CME instituted fewer trading hours on trading days adjacent to Christmas, the Fourth of July, and Thanksgiving.

In 1992, the CME introduced after-hours electronic trading through its Globex trading platform. In 1997, the CME introduced "E-mini" (ES) S&P 500 futures contracts, which are one-fifth the size of regular S&P 500 (SP) futures contracts and trade exclusively on Globex, including during the day. Activity has moved increasingly to electronic trading via Globex, which accounted for 84% of CME group volume by 2011.[4]

The CME provides data in two formats. The "End-of-Day" daily summaries contain open, high, low, close, and settlement prices, as well as volume and open interest, while the transaction-level "Time and Sales" data contain the time and price of every daily transaction in which the price changed from the previous transaction. Bid and ask prices are also recorded in transactions data when the bid price is above or the ask price is below the price of the previous transaction. No information is provided for the pit-traded SP contract regarding the volume of transactions at a particular price, but is provided for the E-minis. I obtained both sets of data for the original full-sized S&P 500 futures SP contract for the period January 3, 1983, to December 31, 2013, and for the entire history of the E-mini ES contract for the period September 7, 1997, to June 30, 2016. I then discarded bid and ask data, as well as transactions that were subsequently cancelled. The 1983 to 2008 SP data are used for parameter estimation, while the 2009 to 2016 E-mini data are used for out-of-sample testing.[5]

[3] The CME and NYSE closed at the same time on October 23 through November 6, 1987, in the aftermath of the 1987 stock market crash.

[4] CME Group, "Twenty Years of CME Globex," June 21, 2012 (http://www.cmegroup.com/education/files/globex-retrospective-2012-06-12.pdf).

[5] Comparison of the end-of-period times of SP and ES trades indicates little difference over the 1998 to 2008 period (12.5 versus 2.5 seconds on average to the end of each 15-minute period), but increasing divergences thereafter. The SP average time gap rose from 25 seconds in 2009 to 135 seconds in 2013, while 15-minute intervals without transactions occurred increasingly frequently: 5 in 2011, 37 in 2012, and 166 in 2013. The ES time gap, by contrast, averaged about 1.4 seconds over 2009 to 2013. Absolute differences between end-of-period SP and ES log futures prices were

S&P 500 futures contracts typically mature on the third Friday of March, June, September, and December—except for March 2008 contracts, which matured a day earlier because of Good Friday. Of the available maturities, I select the shortest maturity with nine or more days until the third Friday, because it is the most actively traded contract according to the "End of Day" volume data. For instance, I use data for March 1983 futures maturing on March 18, 1983, up to the close of trading on Wednesday, March 9. I then use prices of June 1983 contracts to compute overnight futures returns from Wednesday to Thursday, and for intradaily and overnight returns from Thursday, March 10 to the close of trading on Wednesday, June 8.

I construct intradaily 15-minute log-differenced futures prices broadly along the lines of the five-minute futures returns in Chan, Chan, and Karolyi (1991) and Andersen and Bollerslev (1997), by taking the last observed future price in every interval. I use 15-minute returns instead of five-minute returns primarily to triple optimization speed on this large data set, and also to span some short-duration price limit constraints on futures returns over 1989–2002 that I discuss below. For after-hours trading I extend the time window by one minute, typically up through 3:16 PM CST, because trades were often recorded shortly after trading had officially ended. Overnight futures returns are constructed as the difference between the log of the futures price at the end of the first 15-minute trading session (typically 8:30 to 8:45 AM CST) and the log of the futures price of comparable maturity at the end of the preceding day. This approach allows for the incorporation of overnight news into the futures price during the especially volatile initial 15 minutes of trading. Furthermore, skipping the first 15 minutes of trading when computing overnight returns spans possible constraints on opening futures prices from the price limit system instituted by the CME in 1989. The final SP data set contains 6,557 overnight returns and 168,297 intradaily returns from the closing price on December 31, 1982, through December 31, 2008. The 2009 to 2016 E-mini data comprise 1,885 overnight returns and 48,825 intradaily returns.

The CME's price limit system was created in response to the stock market crash of October 19, 1987, and paralleled the NYSE's "circuit breaker" system. The CME's price limits typically involved four prespecified constraints: a relatively tight initial band relative to the previous day's short-maturity S&P 500 futures settlement price that temporarily constrained both upward and downward moves at the open, and three progressively lower price limits (Levels 1 through 3) that temporarily constrained downward moves during the day. Hitting a price limit triggers a specific time interval during which the price limit remains in effect, followed by a two-minute trading halt if the price limit is binding ("locked limit"), followed by the resumption of trading with a new lower price limit in effect. For instance, price change constraints from 1989 to 1996 were 5, 12, 20, and 30 points, respectively, over which time the S&P 500 index rose from 300 to 700. The five-point opening limit lasted only until 8:40,

typically only two to three basis points throughout the 1998 to 2013 period, but were occasionally larger during volatile days or on days adjacent to holidays.

with a trading halt from 8:40 to 8:42 if binding. A 12-point downward move triggered an interval lasting 30 minutes or until 2:30 PM CST, during which time futures contracts could be traded at or above the limit but not below. If the price limit was binding at the end of the interval, a two-minute trading halt was declared, followed by the resumption of trading with the 20-point lower limit in place. Hitting the 20-point downward limit started another interval lasting 30 minutes or until 2:30, followed by a trading halt (if still binding) and the 30-point limit taking effect for the remainder of the day. Separate rules apply if a price limit was binding at the close of the preceding day.

Limits on the opening price change were removed on October 15, 1997 as part of a revision in the circuit breaker system. The levels of permissible downward price changes changed over time, partly because of the rise and fall in the level of the S&P 500. In addition, the price constraints were significantly widened on May 13, 2001 to roughly 5%, 10%, and 15% of the end-of-quarter S&P 500 level, with roughly 20% being the maximal permissible daily price movement. These limits were relaxed further in January 2008 to 10%, 20%, and 30%, respectively, to be consistent with the Dow Jones–based percentages used on the NYSE. (A 5% price limit remained on after-hours trading on Globex.) These revisions in 2001 and 2008 considerably reduced the frequency of trading halts, with an apparent absence of such halts in intradaily data from 2003 to 2008.[6] Even the 10.4% intradaily drop in the December 2008 futures price on October 15, 2008, to 898.5 from October 14's settlement price of 1,002.3 did not exceed the 120-point limit that the CME had set on September 30, 2008, as the 10% limit for the fourth quarter of 2008.

The corresponding time intervals triggered by hitting a price limit were also shortened to roughly 15 minutes in 1996 and to roughly 10 minutes in 1997. However, longer halts could arise because of trading halts at the NYSE. The most notable such incident was the tripping of all three levels of NYSE circuit breakers on October 27, 1997.

Trading at the CME also occasionally halted because of exogenous events in New York or Chicago. On December 27, 1990, for instance, the explosion of a Con Edison transformer in New York delayed the open of the NYSE and CME. On April 13, 1992, the accidental flooding of utility tunnels in Chicago shut down the CME, but not the NYSE.[7] Both the NYSE and CME closed following the attacks on September 11, 2001, and did not reopen until September 17.

Price limits can artificially constrain observed futures returns. Accordingly, I extended the time interval whenever a price limit was hit until that limit had expired and was no longer potentially binding on the futures price. Similarly, I extended time intervals whenever trading was suspended until trading had resumed, and computed returns over the expanded interval. For instance, the

[6] John Nyhoff at the CME kindly provided me with a list of dates and times when the S&P 500 futures price limits were hit during regular trading hours. Stroud and Johannes (2014) note that the Globex-traded E-mini contract hit its overnight limit on October 24, 2008.

[7] A list of market closings at the NYSE is available at http://www.nyse.com/pdfs/closings.pdf. Additional CME trading suspensions were identified by searching the data for periods without reported trades, and matching them against news reports.

CME suspended trading at 11:15 AM CST on October 20, 1987, the day after the 1987 stock market crash,[8] and the December 1987 futures price rebounded when trading resumed at 12:05 PM. I combined returns over 11:15 AM to 12:15 PM into a single one-hour interval, with an associated log-differenced futures price of 13.76%.[9] Over the 1983 to 2008 period, there were 103 instances of expanded time intervals, out of 174,859 total observations. The E-mini data over 2009 to 2016 had three instances of expanded time intervals, out of 50,710 total observations.

B. Models

Affine models allow for considerable flexibility in how diffusive spot variance and jump intensities evolve, and in the interactions between shocks to futures returns and to the underlying state variables. I model the continuous-time process for the log futures price $f_t = \ln F_t$ underlying observed intradaily and overnight S&P 500 futures returns as a potentially multifactor affine jump-diffusion of the form

$$\begin{aligned} df_t &= \mu_0 dt + \sum_{i=1}^{I} \left[(\mu_i - 1/2) V_{it} dt + \sqrt{V_{it}} dW_{it} \right] + \sum_{j=1-K}^{J} \left(\gamma_j dN_{jt} - \lambda_{jt} \bar{k}_j dt \right), \\ dV_{1t} &= (\alpha - \beta_1 V_{1t}) dt + \sigma \sqrt{V_{1t}} dW_{Vt} + \gamma_{V1} dN_{1t}, \\ dV_{it} &= -\beta_i V_{it} dt + \gamma_{Vi} dN_{it} \quad \text{for } i > 1, \end{aligned} \tag{1}$$

where W_{1t} and W_{Vt} are Wiener processes with correlation ρ, W_{it} for $i > 1$ are additional orthogonal Wiener processes, the N_{jt}'s are Poisson counters with stochastic intensity λ_{jt} that depend linearly on the state variables $\boldsymbol{V}_t = (V_{1t}, \ldots, V_{It})'$, and $\bar{k}_j = \mathrm{E}(e^{\gamma_j}) - 1$ is the j^{th} expected percentage jump size in futures. Furthermore, the state variables are divided into a core jump-diffusive variance state variable V_{1t}, and additional pure-jump state variables V_{it} that capture transient variance shocks.

A key empirical question is how many state variables are necessary to adequately summarize the stochastic volatility and jump risks underlying futures returns. Potential specifications are categorized as SVJ(I,J,K) models, where I is the number of underlying state variables, J is the number of synchronous jump processes for futures prices and variance state variables, and $K \leq 1$ is the number of jump processes for futures prices only.

Another important issue is the joint distribution of the (γ_j, γ_{Vj}) cojumps. Affine models require $\gamma_{Vj} \geq 0$ to preclude negative variances, but otherwise

[8] See Carlson (2006, p.11).

[9] Andersen and Bollerslev (1997) follow Chan, Chan, and Karolyi (1991) in omitting data over October 15 through November 13, 1987. They also linearly interpolate prices when data are missing, yielding roughly identical successive five-minute returns.

place no restrictions on this joint distribution. I use the Duffie, Pan, and Singleton (2000) specification

$$\gamma_j = \rho_j \gamma_{Vj} + \gamma_{fj}, \tag{2}$$

where $\gamma_{Vj} \sim \text{Exp}(\bar{\gamma}_{Vj})$ is the exponentially distributed jump in spot variance V_{jt} conditional on $dN_{jt} = 1$, $\gamma_{fj} \sim N(\bar{\gamma}_{fj}, \delta_{fj}^2)$ is an independent Gaussian shock, and ρ_j captures the degree to which synchronous jumps in futures prices and variance covary. The Poisson counter N_{0t} identifies additional futures price jumps (with a V_{1t}-sensitive jump intensity) that are unaccompanied by volatility jumps—an extension that substantially improves overall fit. Volatility jumps that are unaccompanied by price jumps are also possible if $(\rho_j, \bar{\gamma}_{fj}, \delta_{fj}^2) = 0$.[10]

The final empirical issue is the specification of jump intensities. Whereas Duffie, Pan, and Singleton (2000) is a constant-intensity model, self-exciting jumps are plausibly a major explanation for the intradaily development of major daily outliers.[11] For tractability, I use jump intensities of the general form

$$\lambda_{jt} = \begin{cases} \lambda_{j0} + \lambda_{j1} V_{1t^*} & \text{for } j \leq 1 \\ \lambda_{j0} + \lambda_{j1} V_{1t^*} + \lambda_{jj} V_{jt^*} & \text{for } j > 1, \end{cases} \tag{3}$$

with specific parameter restrictions discussed further below. The jump intensities λ_{jt} for each Poisson counter N_{jt} are assumed to be constant within each intradaily or overnight period, reset at the end of every period, and depend on the spot variance levels $\boldsymbol{V}_{t^*}$ prevailing at the start of the period. This allows jumps to be self-exciting across periods while retaining the analytic tractability of the Duffie, Pan, and Singleton (2000) model. The recursive structure in (3) for $j > 1$ allows the initiation of additional self-exciting volatility components V_{jt} to depend on the level of core volatility V_{1t}.

The multifactor specification for $\boldsymbol{V}_t$ in equations (1) to (3) allows for considerable flexibility in how underlying diffusive variances and jump intensities can evolve. For instance, the multifactor specification (1) nests a univariate model with variance jumps drawn from a mixture of exponentials, when the rates of mean reversion β_i are identical and jump intensities are similarly restricted. More generally, multivariate models allow the distributions of jumps in stock market returns and in total diffusive spot variance to vary as the components of $\boldsymbol{V}_t$ change. Those components can have different degrees of persistence, and different correlations with the contemporaneous stock market returns from which they are estimated. Because each V_{it} follows an independent AR(1) process, total diffusive variance and jump intensities follow ARMA(I, $I-1$) processes.

[10] Andersen, Fusari, and Todorov (2015) propose an interesting but less tractable model in which the futures jump γ_j has a double exponential distribution. Variance jumps are a weighted sum of the negative price jump component squared and an additional independent squared exponential shock.

[11] See Fulop, Li, and Yu (2015) for estimates of such a model from daily stock index returns.

The model does not explicitly consider scheduled announcement effects, which Prokopczuk and Semen (2014) estimate at 25% of observed jumps in E-mini futures prices during regular business hours over the period 2008 to 2014.[12] Major macroeconomic announcements are treated as randomly timed jumps, with the schedule unexploited in specification (3) of jump intensities. Furthermore, the estimates below implicitly assume that such announcements have the same self-exciting dynamic implications of other jumps. Stroud and Johannes (2014) provide a detailed look at the volatility impact of various major scheduled announcements, most of which are deliberately scheduled outside of regular trading hours.

Affine models such as equations (1) to (3) imply that the joint cumulant-generating function of returns $y_{t+1} = f_{t+1} - f_t$ and future spot variances $\boldsymbol{V}_{t+1}$ given current $\boldsymbol{V}_t$ is affine in $\boldsymbol{V}_t$,

$$\begin{aligned} CGF\ (\Phi, \boldsymbol{\psi} | \boldsymbol{V}_t,\ \tau_t) &= \ln \mathrm{E}\left[\mathrm{e}^{\Phi y_{t+1} + \boldsymbol{\psi}' \boldsymbol{V}_{t+1}} \mid \boldsymbol{V}_t\right] \\ &= C\left(\tau_t; \Phi, \boldsymbol{\psi}\right) + \boldsymbol{D}(\tau_t; \Phi, \boldsymbol{\psi})' \boldsymbol{V}_t, \end{aligned} \tag{4}$$

where τ_t is the time horizon. The precise functional forms of $C(\cdot)$ and $\boldsymbol{D}(\cdot)$ for the various SVJ(I,J,K) models are in Appendix A. By iterated expectations, the joint conditional cumulant-generating function conditional on observing past data $\boldsymbol{Y}_t = \{y_1, \ldots, y_t\}$ is then of the form

$$\begin{aligned} CGF\ (\Phi, \boldsymbol{\psi} | \boldsymbol{Y}_t,\ \tau_t) &= \ln \mathrm{E}\left\{\exp\left[\Phi y_{t+1} + \boldsymbol{\psi}' \boldsymbol{V}_{t+1}\right] \mid \boldsymbol{Y}_t\right\} \\ &= C\left(\tau_t; \Phi, \boldsymbol{\psi}\right) + g_{t|t}\left[\boldsymbol{D}(\tau_t; \Phi, \boldsymbol{\psi})\right], \end{aligned} \tag{5}$$

where $g_{t|t}(\boldsymbol{\psi}) \equiv \ln \mathrm{E}[e^{\boldsymbol{\psi}' \boldsymbol{V}_t} | \boldsymbol{Y}_t]$ is the cumulant-generating function of $\boldsymbol{V}_t$ conditional on data $\boldsymbol{Y}_t$. I discuss below in more detail how to compute $g_{t|t}(\boldsymbol{\psi})$ recursively via Bayesian filtration.

C. Rounding Models and Filtration

Because SP S&P 500 futures had a price tick size of 0.05 through October 31, 1997, and 0.10 thereafter, observed intradaily futures returns are not drawn from a continuous distribution. Indeed, 5% of all intradaily 15-minute returns over 1983 to 2008 are exactly zero despite intervening intraperiod price changes,[13] while 42% are over a range of ±5 price ticks. The E-minis had a tick size of 0.25 throughout 1997 to 2016, and 42% of E-mini absolute price changes were zero to three price ticks over 2009 to 2016. Consequently, the above continuous-time models are assumed to represent the

[12] Prokopczuk and Simen (2014) use a Lee and Mykland (2008) nonparametric jump estimation procedure at a five-minute frequency, with adjustments for diurnal effects. They find that another 25% of jumps are attributable to major but unscheduled news, with the remaining 50% unassociated with any observable news. They also find that unscheduled jumps have three times the overall variance contribution of scheduled jumps.

[13] On average there were 30 price changes per period for those intradaily periods with a futures return of zero.

underlying conditional distribution of futures returns, and those returns are rounded to the futures returns actually observed. I compute the scaled probability of an observed log futures return $y_{t+1} = \ln(F_{t+1}/F_t)$ over a horizon of length τ_t via Fourier inversion as the integrated conditional density of all realizations falling within $\pm$½ of a price tick of the observed F_{t+1}:

$$P_{t+1} = \frac{\text{Prob}[y_{t+1} \in (\underline{y}_{t+1}, \bar{y}_{t+1}) | \boldsymbol{Y}_t]}{\bar{y}_{t+1} - \underline{y}_{t+1}}$$

$$= \frac{1}{2\pi} \int_{-\infty}^{\infty} e^{C(\tau_t; i\Phi, 0) + g_{t|t}[\boldsymbol{D}(\tau_t; i\Phi, 0)]} \frac{e^{-i\Phi\bar{y}_{t+1}} - e^{-i\Phi\underline{y}_{t+1}}}{-i\Phi\left(\bar{y}_{t+1} - \underline{y}_{t+1}\right)} d\Phi \quad \text{for } \underline{y}_{t+1}$$

$$= \ln\left(\frac{F_{t+1} - \varepsilon/2}{F_t}\right), \quad \bar{y}_{t+1} = \ln\left(\frac{F_{t+1} + \varepsilon/2}{F_t}\right), \text{ and } \varepsilon = \text{one price tick.} \quad (6)$$

I then estimate parameters by maximizing the log likelihood function $\ln L = \sum_t \ln P_{t+1}$.[14] The computed probabilities are scaled by $\bar{y}_{t+1} - \underline{y}_{t+1}$ to make the results comparable in magnitude to log likelihood values based on conditional probability densities.

The conditional moment generating function $G_{t|t}(\boldsymbol{\psi}) = \exp[g_{t|t}(\boldsymbol{\psi})]$ that summarizes what is known about $\boldsymbol{V}_t$ at time t can be updated recursively over time via a straightforward extension of the AML methodology in Bates (2006, 2012):

$$G_{t+1|t+1}(\boldsymbol{\psi}) = \frac{1}{2\pi P_{t+1}} \int_{-\infty}^{\infty} e^{C(\tau_t; i\Phi, \boldsymbol{\psi}) + g_{t|t}[\boldsymbol{D}(\tau_t; i\Phi, \boldsymbol{\psi})]} \frac{e^{-i\Phi\bar{y}_{t+1}} - e^{-i\Phi\underline{y}_{t+1}}}{-i\Phi(\bar{y}_{t+1} - \underline{y}_{t+1})} d\Phi. \quad (7)$$

Derivatives of equation (7) provide the noncentral posterior moments of $\boldsymbol{V}_{t+1}$ conditional on adding the latest datum y_{t+1} to the data set,

$$\mathrm{E}\left[V_{i,t+1}^n | \boldsymbol{Y}_{t+1}\right] = \left.\frac{\partial^n G_{t+1|t+1}(\boldsymbol{\psi})}{\partial \psi_i^n}\right|_{\boldsymbol{\psi}=0}, \quad (8)$$

using analytical derivatives of the integrand in equation (7). These posterior moments are used to generate a gamma-based moment matching approximation to $g_{t+1|t+1}(\boldsymbol{\psi})$ of the form

$$g_{t+1|t+1}(\boldsymbol{\psi}) = -\sum_{i=1}^{I} v_{i,t+1} \ln\left(1 - \kappa_{i,t+1}\psi_i\right), \quad (9)$$

where

$$\mathrm{E}\left[V_{i,t+1} | \boldsymbol{Y}_{t+1}\right] \equiv \hat{V}_{i,t+1|t+1} = \kappa_{i,t+1}\, v_{i,t+1},$$

$$\mathrm{Var}\left[V_{i,t+1} | \boldsymbol{Y}_{t+1}\right] \equiv P_{i,t+1|t+1} = \kappa_{i,t+1}^2\, v_{i,t+1}. \quad (10)$$

[14] This approach generalizes the Gaussian ordered-probit approach of Hausman, Lo, and MacKinlay (1992) to arbitrary underlying distributions (5). See Campbell, Lo, and MacKinlay (1997, Section 3.3.2) and Aït-Sahalia and Jacod (2014, Section 2.3.2) for overviews of rounding models.

The overall procedure is a version of robust Kalman filtration and directly generates filtered estimates $\hat{\boldsymbol{V}}_{t|t}$ of the latent state variables as a by-product.[15]

The realized variance literature has focused on nonparametric estimation of the diffusive variance and jump components of intraperiod quadratic variation. In an affine model, these quantities are affine latent variables that can be directly estimated from observed futures returns, in the same fashion as in equations (7) and (8) above for estimating latent $\boldsymbol{V}_{t+1}$. In Appendix A, I derive the relevant versions of $C(\cdot)$ and $\boldsymbol{D}(\cdot)$ to compute $\mathrm{E}[\Delta x_{t+1}|\boldsymbol{Y}_{t+1}]$ for various latent characteristics x_t of interest. This filtration procedure is similar to that in Lee and Mykland (2008) in using only past and current data to estimate diffusive variance and jumps for every period.[16]

D. *Intradaily and Overnight Seasonals*

The effective length of any time interval differs for overnight and intradaily 15-minute returns. In addition, there is intradaily variation in trading activity and volatility, as well as day-of-the-week effects for intradaily and overnight effects. Finally, the actual length of a given trading day occasionally varies because of late openings or early closings—especially the half-day trading that began in December 1990 on specific days adjacent to Christmas, the Fourth of July, and Thanksgiving.

I arbitrarily select Wednesday as the benchmark day, with Tuesday close to Wednesday close representing one full business day. The effective division between overnight returns (including the first 15 minutes of intradaily market trading) and intradaily returns (for the remainder of the day, typically until 3:16 PM CST) is estimated as variance proportions $(1 - f_{daily}, f_{daily})$, respectively. I construct the daily time horizon 252 τ_{nm} on day n and time segment m as

$$252\tau_{nm} = \begin{cases} (1 - f_{daily}) \exp(\boldsymbol{\beta}_{ON}{}' \boldsymbol{d}_n^{ON}) \text{ overnight } (m = 0) \\ f_{daily} \frac{\exp[f(m,M_n)]}{\sum_{m=1}^{M_n} \exp[f(m,M_n)]} \exp\left(\boldsymbol{\beta}_{ID}{}' \boldsymbol{d}_n^{ID}\right) \text{ intradaily } (m > 0) \\ 5 - f_{daily} \exp\left(\beta_{Monday}\right) \text{ for Sept. 10 to 17, 2001 (close to open),} \end{cases} \tag{11}$$

where $\boldsymbol{d}_n^{ON}$ are day-of-the-week, holiday, and weekend dummies for overnight returns, $\boldsymbol{d}_n^{ID}$ are day-specific dummies for intradaily returns (including a half-day indicator for shortened trading days adjacent to holidays), and $M_n \leq 26$ is the number of 15-minute segments available on day n after the opening segment.

[15] Bates (2006) shows that AML parameter estimation efficiency is comparable to that of the Monte Carlo Markov Chain (MCMC) approach, for specific stochastic volatility processes with and without jumps. MCMC generates smoothed but not filtered estimates of latent state variables.

[16] Tauchen and Zhou (2011) and Andersen, Fusari, and Todorov (2015) by contrast use nonparametric smoothing procedures. All five-minute returns in a given day are used to identify jumps at any time within that day.

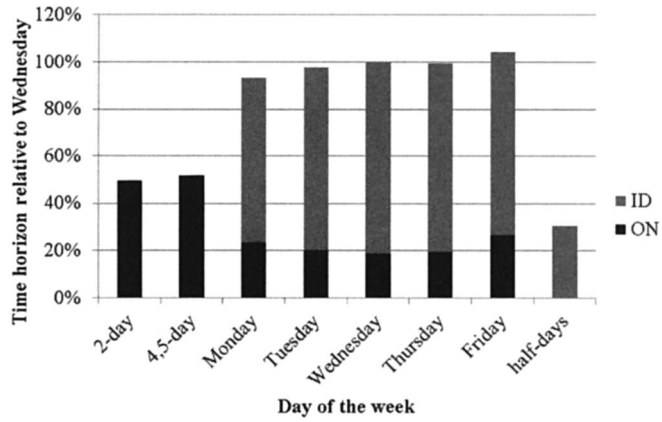

Figure 1. Overnight (ON) and intradaily (ID) time horizons, relative to Wednesday (from Tuesday close to Wednesday close). Overnight returns for Monday (from Friday close to Monday open) and for Tuesday through Friday include the first 15 minutes of the opening day, as do overnight returns spanning two-day holidays and four- or five-day holiday weekends. (Color figure can be viewed at wileyonlinelibrary.com)

The function $f(m, M_n)$ follows Andersen and Bollerslev (1997) in using Gallant's (1981) flexible Fourier form approach to estimate the intradaily variance pattern

$$f\ (m, M_n)\ = b_1 \frac{m}{\mathrm{Avg}_n\,(m)} + b_2 \frac{m^2}{\mathrm{Avg}_n\,(m^2)} + b_{ah} 1\,(m\ =\ ah) + \sum_{p\,=\,1}^{2} \left[c_p \cos\left(2\pi\, p \frac{m}{M_n}\right) + d_p \sin\left(2\pi\, p \frac{m}{M_n}\right) \right], \tag{12}$$

where $\mathrm{Avg}_n\,(m) = (M_n\ + 1)/2$, $\mathrm{Avg}_n\,(m^2) = (M_n\ + 1)(M_n + 2)/6$, and $1(m\ =\ ah)$ indicates an after-hours trading segment at $m\ = M_n$.[17]

As discussed above, intradaily futures returns were constrained by endogenous price limits or exogenous market closings on 103 occasions over the 1989 to 2002 period. In such cases, I aggregate log futures returns over additional periods until the trading constraint or market closing is no longer in effect, and I treat the yearly time interval associated with that aggregate log return as the sum of the spanned τ_{nm}'s. This approach is equivalent when filtering $\boldsymbol{V}_t$ to treating the subintervals of the full interval as missing observations.

Figure 1 shows the Vjump1b estimates of the intradaily and overnight variance patterns.[18] Overnight trading (including trading in the first 15 minutes of Wednesday morning) typically accounts for 18.8% of the return variance from Tuesday close to Wednesday close. Intradaily trading over the remainder

[17] There were no after-hours sessions from October 23 to November 6, 1987.

[18] Because the results from other one-factor models are almost identical, I also use the Vjump1b time parameter estimates in the multifactor Vjump2 and Vjump3 models, to speed up optimization.

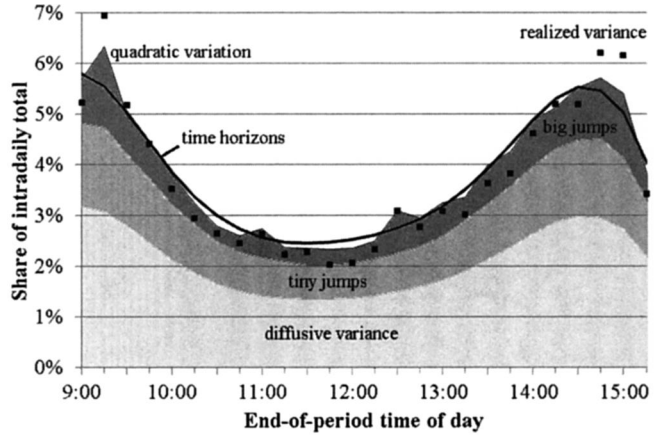

Figure 2. Estimated intradaily 15-minute horizons and quadratic variation over 1985 to 2008, as percentages of the intradaily totals. The shaded areas indicate the period-specific estimated components of quadratic variation from the Vjump1b model. The black rectangles are period-specific realized variances as percentages of total intradaily estimated quadratic variation.

of Wednesday accounts for the remaining 81.2%. These patterns are roughly comparable for other days of the week. As shown in Figure 1, there is a U-shaped weekly pattern to overnight return variance and an inverse U-shaped pattern to intradaily variance, with the sum of the two imparting a roughly flat but slightly increasing trend in business day variance across the week. Holidays during the week or as part of a holiday weekend substantially increase the variance of "overnight" returns that span those holidays. Intradaily trading on half-days adjacent to holidays have only 37.5% the variance of a regular intradaily trading interval.

Figure 2 shows the intradaily pattern of effective time horizons for 15-minute returns over 8:45 AM through 3:16 PM for the longer trading days on September 30, 1985 through December 31, 2008, excluding the initial 8:30 to 8:45 interval. For comparison, period-specific average filtered quadratic variations and their diffusive variance, tiny jump, and big jump components from the Vjump1b model are also plotted, as are period-specific realized variances observed over 1985 to 2008. The roughly U-shaped intradaily pattern in time horizons roughly reflects the intradaily pattern of realized variance. Average filtered quadratic variation is approximately but not exactly equal to average realized variance, with diffusive variance and tiny jump components responsible for 85% of the total intradaily quadratic variation. The realized variance and big jump outliers in the second 9 to 9:15 period appear attributable to large 3.5% to 5% drops in the stock market on October 19, 20, and 22, 1987, rather than to regularly scheduled announcements at 9 AM CST.[19]

The U-shaped pattern in time horizons and realized variances mimics Andersen and Bollerslev's (1997) Figure 6b, which is estimated on five-minute

[19] Andersen and Bollerslev (1998) find pronounced announcement effects evident in five-minute currency returns at 9 to 9:05 AM CST.

S&P 500 futures returns using a GARCH model. Variance peaks in the afternoon at 2:15 to 2:30 PM CST and falls off thereafter, especially in the after-hours 3 to 3:15 PM trading segment. Andersen and Bollerslev (1997) emphasize that it is critical to account for this periodic intradaily pattern, which if ignored would strongly affect estimates of variance mean reversion. Accounting for this intradaily periodicity is also important when estimating jump risk. Substantial distributional mixing occurs, with opening and closing returns having roughly double the variance (40% higher volatility) of midday returns. Failing to account for this mixing would exaggerate the conditional leptokurtosis of 15-minute returns and increase the estimated magnitudes of intradaily jump risk.

E. Volatility and Jump Parameter Estimates

Tables B.I to B.V in Appendix B contain estimates of the other jump-diffusion parameters that describe the evolution of diffusive spot variances $\boldsymbol{V}_t$ and the distributions of jumps. Five models are considered, all sequentially nested:

Model	Variance processes	Jumps in log futures prices
SVJ1	One-factor diffusive process for V_{1t}; no volatility jumps	Normally distributed jumps with V_{1t}-dependent jump intensity
Vjump1a	One-factor jump-diffusion	Jumps are correlated with V_{1t} jumps and have a V_{1t}-dependent jump intensity
Vjump1b	One-factor jump-diffusion	Two jumps: one uncorrelated with V_{1t} jumps, one correlated. Both have V_{1t}-dependent intensities
Vjump2	Two-factor additive variance process. V_{1t} follows a jump-diffusion, while V_{2t} is a pure-jump volatility spike process	Three jumps, with the last two correlated with V_{1t} and V_{2t} jumps, respectively
Vjump3	Three-factor additive variance process. V_{1t} follows a jump-diffusion, while V_{2t} and V_{3t} are pure-jump volatility spike processes	Four jumps, with the last three correlated with V_{1t}, V_{2t}, and V_{3t} jumps, respectively

I estimate all of the above models with the constraint $\lambda_{j0} = 0$ for $j \leq 1$, based on evidence in Bates (2006, Table 7) supporting that restriction.[20] In addition, I estimate the models Vjump20 and Vjump30 with $\lambda_{j0} \neq 0$ for $j \leq 1$ and with the self-exciting jump components suppressed by setting $\lambda_{jj} = 0$ for all $j \geq 1$.

Comparing the models in Table B.I and in Figure 3 points to two important sources of overall improvement in fit. The first relates to accurately modeling high-frequency price changes of zero to five ticks, which account for 42% of the data. Of primary importance is the introduction in model Vjump1b of a second futures jump component N_{0t} that is uncorrelated with variance jumps. This

[20] Relaxing this constraint for the Vjump3 model raises the log likelihood from 893,432.73 to 892,438.82—a small but statistically significant change.

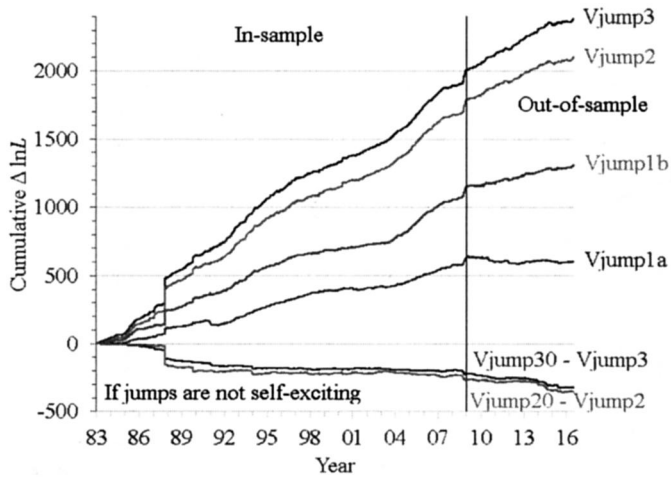

Figure 3. Cumulative log likelihood improvements relative to the one-factor SVJ1 model, and impact of eliminating self-exciting jumps in the Vjump2 and Vjump3 models. (Color figure can be viewed at wileyonlinelibrary.com)

futures jump component is estimated as a high-frequency, small-amplitude jump component in Vjump1b, and is even higher in frequency and smaller in amplitude in the more general Vjump2 and Vjump3 models (Table B.IV). While observationally equivalent for daily returns to just scaling up diffusive variance V_{1t}, the N_{0t} futures jump component helps model the 15-minute price changes of zero to five ticks more precisely. The adjusted correlation parameter

$$\rho^{adj} \equiv \frac{\rho + \rho_1 \lambda_{11} \mathrm{E}\left(\gamma_{V1}^2\right)}{\sqrt{\sigma^2 + \lambda_{11} \mathrm{E}\left(\gamma_{V1}^2\right)}\sqrt{1 + \lambda_{01} \mathrm{E}\left(\gamma_0^2\right) + \lambda_{11} \mathrm{E}\left(\gamma_1^2\right)}} \tag{13}$$

in Table B.III indicates the overall leverage effect—the equivalent of $\rho = \mathrm{Corr}(dW_{1t}, dW_{Vt})$ if the $(\gamma_0, \gamma_1, \gamma_{V1})$ shocks were replaced by diffusive shocks with equivalent variances and covariances.

The second major source of improvement in fit is the impact of the 1987 crash. Better modeling of intradaily developments on October 19 and 20 accounts for almost a quarter of the log likelihood improvement in-sample of the most general Vjump3 model versus SVJ1 in Figure 3. The more general models also fit data in the fall of 2008 progressively better, indicating that the two largest stock market crises in the 1983 to 2008 period substantially influence parameter estimates. Turbulent markets at other times (the first Gulf War, market declines in 1997 and 1998, and post-9/11) do not appear to have had as much of an impact on log likelihood fits. However, log likelihoods are generally increasing throughout the full 1983 to 2008 sample.

The more general models also fit better out-of-sample over 2009 to 2016. The progressively better fit of the Vjump1b, Vjump2, and Vjump3 models out-of-sample is entirely attributable to better modeling of zero to three tick

price movements, which account for 42% of observed E-mini price changes. Further breakdown in Table B.II by volatility environment indicates that these models fit all data better regardless of the recent level of realized volatility, both in-sample and out-of-sample. The Vjump20 and Vjump30 models without self-exciting jumps do worse both in-sample (mostly during the 1987 crash) and out-of-sample.

The multifactor Vjump2 and Vjump3 models have progressively richer descriptions of variance dynamics relative to the nested Vjump1b model. In particular, these two models indicate that substantial self-exciting volatility spikes are an important component of volatility evolution. In the Vjump2 estimates, V_{2t} is typically near zero and has a V_{1t}-dependent intensity that averages out to $\lambda_{20} + \lambda_{21}\mathrm{E}(V_{1t}) = 48$ jumps per year. If a variance jump occurs of average size 0.07, V_{2t} increases to $(0.265)^2$ and the jump intensity increases by $\lambda_{22}\,\bar{\gamma}_{V2} = 1{,}486$ jumps per year, or six jumps per day. This increase in jump intensity implies that $\lambda_{22}\bar{\gamma}_{V2}/(\beta_2 - \lambda_{22}\bar{\gamma}_{V2}) = 3.0$ additional variance jumps are expected from every average-sized jump in V_{2t}.[21] Furthermore, the positively skewed exponential distribution can have V_{2t} jumps that are two or three times the average jump magnitude $\bar{\gamma}_{V2}$, with corresponding projections of six or nine additional variance jumps. The associated futures price jumps have roughly zero mean, a standard deviation of 0.36%, and a strongly negative correlation (-0.92) with the variance jumps. The V_{2t} spikes resulting from variance jumps are highly transient, with an estimated half-life of roughly one-third of a day.

The Vjump3 model decomposes variance jumps into small, medium, and large sizes, with different properties and different associations with the futures returns from which they are filtered. The moderately frequent V_{2t} jumps of average size 0.070 in the Vjump2 model are further divided in the Vjump3 model into frequent jumps in V_{2t} of average size 0.022 and rarer jumps in V_{3t} with average size 0.076. The V_{2t} jumps have little self-propagation, die off rapidly within the day (half-life of 0.08 days), and primarily add additional and transient noise to the combined spot variance process $V_{1t} + V_{2t}$. The large and relatively rare V_{3t} jumps have a -0.76 correlation with associated log futures jumps $\gamma_3 \sim [-0.2\%,\ (1.0\%)^2]$, indicating that they are inferred from the largest 15-minute or overnight futures returns. V_{3t} reverts toward zero with a half-life of 1.6 days, implying some spillover across days. Sequences of V_{3t} jumps typically initiate from near zero values of V_{3t}, with a V_{1t}-dependent intensity that averages out to $\lambda_{30} + \lambda_{31}\mathrm{E}(V_{1t}) = 7.4$ jumps per year. Conditional on initiation, each average-sized V_{3t} jump generates an expected additional 4.9 jumps through its impact on expected future jump intensities.

Let V_{it}^{tot} be the total impact of the state variable V_{it} on diffusive and jump variance, using the variance factor loadings of Table B.V. Figure 4 graphs the incremental contributions of the total variance components to end-of-day

[21] This calculation is based on a continuous-time stochastic intensity $\lambda_{2t} = \lambda_{20} + \lambda_{21}V_{1t} + \lambda_{22}V_{2t}$, with reversion rate $\beta_2 - \lambda_{22}\bar{\gamma}_{V2}$ for V_{2t}. The increase in expected future jumps (from an increase in expected future jump intensities) is approximately equal to but less than the number when jump intensities are constant within periods.

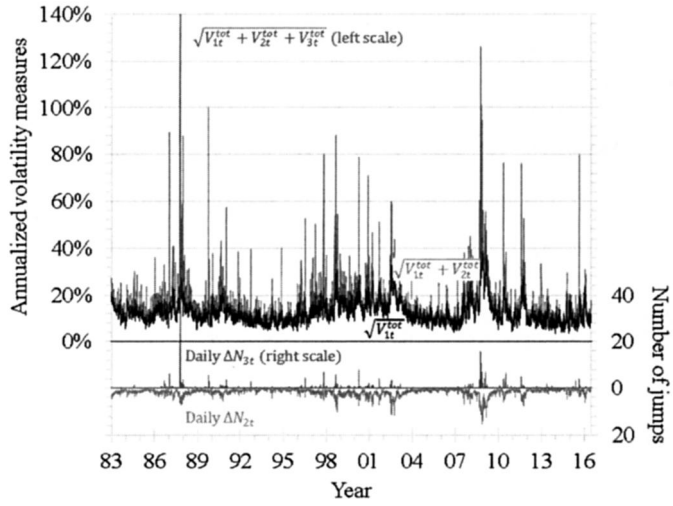

Figure 4. Components of annualized conditional volatility and daily estimated number of jumps, 1983 to 2016. Total end-of-day variance estimates V_{it}^{tot} from the three-factor variance model Vjump3 include the contributions to both diffusion risk and jump risk. (Color figure can be viewed at wileyonlinelibrary.com)

total spot volatility $(V_{1t}^{tot} + V_{2t}^{tot} + V_{3t}^{tot})^{1/2}$ over the 1983 to 2016 period. The total estimated number of jumps each day (from close to close), calculated using the filtration procedure described in Section I.C above, is also shown. Figure 4 indicates that major but substantially transient volatility spikes from V_{3t} jumps tend to occur when core volatility $\sqrt{V_{1t}^{tot}}$ is relatively high. Furthermore, the volatility spikes are typically the outcome of *multiple* synchronous jumps in log futures prices and underlying volatility. For instance, the −32.7% change in the log futures price on October 19, 1987, from the previous Friday's closing value was the result of an estimated 34 jumps in V_{3t}. Similarly, the +5.7% and +17.4% returns on October 20 and 21 were the outcome of 97 and 52 jumps, respectively, in V_{3t}. The turbulent and predominantly falling market in the fall of 2008 was the result of multiple intradaily and overnight jumps in V_{2t} and V_{3t} that accompanied predominantly negative stock market jumps.

Figure 5 shows the intradaily evolution of the three factors over October 12 to 30, 1987. A declining stock market over the week of October 12 to 16, including an accelerating drop on Friday, October 16, set the stage for the stock market crash of October 19. A volatility spike began developing late on Friday afternoon, and was further stimulated by the log futures price dropping 5.4% by 9:15 AM on Monday, October 19. Substantial intradaily drops over October 19 generated additional substantial estimated increases in the volatility spike factor $\sqrt{V_{3t}^{tot}}$, which ended the day at roughly 193% annualized (2.1% per quarter-hour). Major market turbulence on October 20 contributed to further estimated increases in $\sqrt{V_{3t}^{tot}}$, which peaked at 282% annualized (3.1% per quarter-hour) at midday before ultimately declining in the afternoon and on October 21. Log futures prices fell 5% between 9 and 9:15 AM on October 22,

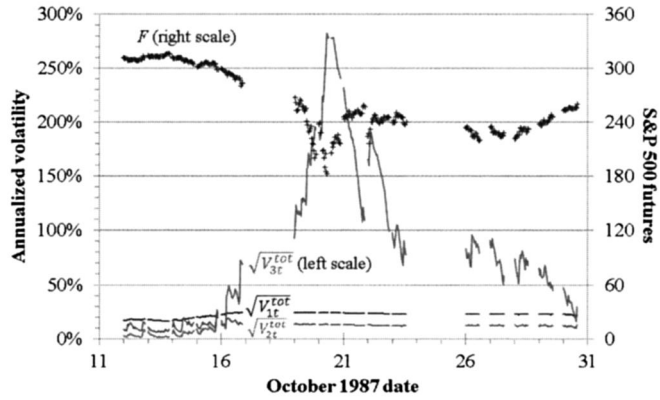

Figure 5. Annualized intradaily conditional volatility factors over October 12 to 30, 1987 (100% annualized = 1.1% per quarter-hour). The December 1987 S&P 500 futures price (+) is on the right scale. (Color figure can be viewed at wileyonlinelibrary.com)

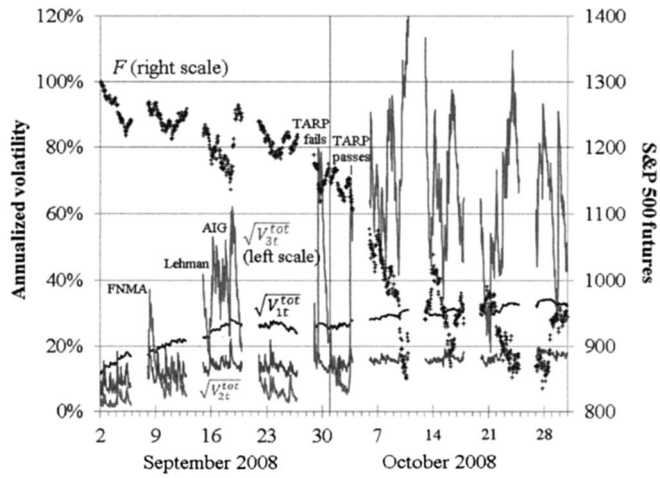

Figure 6. Annualized intradaily conditional volatility factors over September and October 2008 (100% annualized = 1.1% per quarter-hour). September and December 2008 S&P 500 futures prices (+) are on the right scale. (Color figure can be viewed at wileyonlinelibrary.com)

prompting another short-lived volatility burst that decayed as the market rebounded and stabilized.

Figure 6 shows the comparable evolution in factors over September and October 2008. The sharp shocks to the volatility spike factor $\sqrt{V_{3t}^{tot}}$ in September largely reflect various announcements: the government takeover of FNMA and FHLMC announced on September 7, the Lehman Brothers bankruptcy declaration before markets opened on September 15, and the Senate's initial rejection of the Troubled Asset Relief Program (TARP) on September 29. Interestingly, the subsequent passage of TARP on October 3 also caused a decline in the market, and an associated jump in $\sqrt{V_{3t}^{tot}}$. The House of Representatives' vote

to approve TARP at 1:27 EST was accompanied by a −0.74% drop in futures prices over 12:15 to 12:30 CST, and a further decrease of −1.76% by 12:45. $\sqrt{V_{3t}^{tot}}$ rose immediately in response, from 5.7% to 9.2% to 44.2% annualized over 12:15 to 12:45. A declining market for the remainder of the day kept $\sqrt{V_{3t}^{tot}}$ high throughout the afternoon. The subsequent week of October 6 to 10 saw a further market decline of 20% and associated high values of volatility. The market remained turbulent throughout the remainder of October.

F. Return Diagnostics

Whether the above models are broadly capturing the conditional distributions of returns can be examined by looking at the normalized returns $z_{t+1} = N^{-1}[\text{CDF}(y_{t+1}|\boldsymbol{Y}_t, \hat{\Theta})]$, where CDF$(\cdot)$ is the conditional cumulative distribution function derived from the specified models and computed by Fourier inversions involving the associated conditional characteristic functions. Under correct model specification, these residuals are independent draws from a standard Gaussian distribution. Table I reports in-sample summary statistics for z's from various models, while Figure 7 presents related normal probability plots. Normalized returns are computed at two horizons: for intradaily/overnight returns conditional on past data, and for daily returns (from close to close) conditional on past intradaily and overnight data up through the close of the preceding day. In addition, 100 sample paths of data over 1983 to 2008 were simulated at the estimated parameters and time horizons, and were used to generate 95% confidence intervals for Figure 7.

Table I and Figure 7 indicate that the multifactor models are doing a progressively better job in-sample of capturing conditional distributions at the intradaily/overnight frequencies used when estimating the models. The first four moments are roughly those of a standard normal distribution, although there are statistically significant deviations in all cases. The graphs in the first column of Figure 7 show that the multifactor models Vjump2 and Vjump3 help capture intradaily outliers, which are often substantially sequential. Both models do well for $|z|$-values less than four, but have some difficulty in capturing the extreme tails ($|z| > 4$). The Vjump2 model underpredicts extreme negative returns, while the Vjump3 model overpredicts those returns. Both models underpredict extreme positive returns ($z > 4$).

The statistics in Table I for daily data indicate that the one-factor variance models Vjump1a and Vjump1b have difficulty capturing the stock market crash of October 19, 1987. Whereas the Vjump1b model partially explains any single 15-minute intradaily outlier, the probability under that model of observing the sequence of outliers that culminated in the overall −32.7% change in log futures prices is low—the equivalent of observing a seven standard deviation draw from a standard normal distribution. By contrast, the two-factor model Vjump2 successfully captures the 1987 outlier as a volatility spike that is plausible under the (in-sample) parameter estimates. The Vjump3 model does even better at capturing that one day.

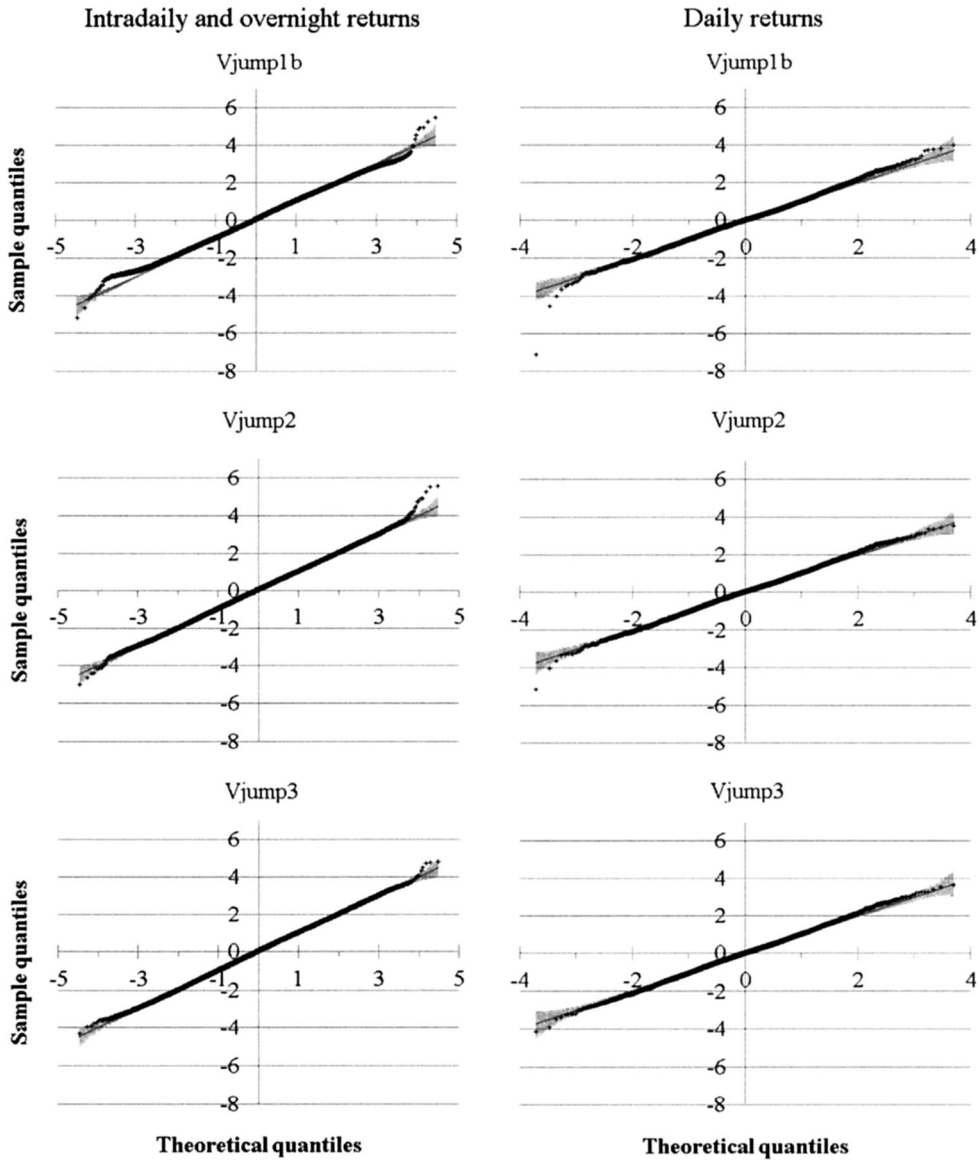

Figure 7. Normal probability plots for various models. Panels in the first column compare the ordered normalized residual values $z_{t+1} = N^{-1}[\text{CDF}(y_{t+1}|\boldsymbol{Y}_t, \hat{\Theta})]$ (+ symbols on the vertical axis) with the models' predicted values (diagonal lines) over 1983 to 2008. The second column does the same for daily returns conditional on intradaily and overnight data $\boldsymbol{Y}_t$ through the end of the preceding day. Gray areas show 95% confidence intervals from 100 simulated paths. (Color figure can be viewed at wileyonlinelibrary.com)

Table I

Statistical Properties of the Normalized Returns for Parameter Estimates from Various Models

This table presents summary statistics for the normalized returns $z_{t+1} = N^{-1}[\text{CDF}(y_{t+1}|Y_t, \hat{\Theta})]$ at intradaily/overnight and daily frequencies. Under correct model specification, the z_{t+1} values should be independent draws from a Gaussian $N(0, 1)$ distribution. Heteroskedasticity-consistent standard errors are in parentheses

	Vjump1a	Vjump1b	Vjump2	Vjump3
Intradaily and overnight returns (174,854 observations)				
Maximum	6.49	5.46	5.54	4.79
Minimum	−7.38	−5.17	−5.01	−4.41
Mean	0.064	0.063	0.053	0.050
(Std. error)	(0.002)	(0.002)	(0.002)	(0.002)
Std. deviation	0.956	0.970	0.999	1.001
Skewness	0.03	0.01	−0.01	−0.02
Excess kurtosis	−0.11	−0.20	0.02	0.00
Corr(z_{t+1}, z_t)	−0.013	−0.015	−0.012	−0.013
(Std. error)	(0.003)	(0.002)	(0.002)	(0.002)
Corr($\|z_{t+1}\|, \|z_t\|$)	0.016	0.025	0.006	−0.005
(Std. error)	(0.003)	(0.003)	(0.002)	(0.002)
Daily returns (6,558 observations)				
Maximum	4.10	3.99	3.54	3.65
Minimum	−7.39	−7.11	−5.17	−4.16
Mean	0.004	0.013	0.019	0.005
(Std. error)	(0.013)	(0.013)	(0.013)	(0.013)
Std. deviation	1.051	1.037	1.028	1.032
Skewness	0.01	0.03	0.00	0.04
Excess kurtosis	0.79	0.53	0.17	0.24
Corr(z_{t+1}, z_t)	−0.004	−0.006	−0.004	−0.010
(Std. error)	(0.012)	(0.012)	(0.012)	(0.012)
Corr($\|z_{t+1}\|, \|z_t\|$)	−0.070	−0.068	−0.070	−0.067
(Std. error)	(0.012)	(0.012)	(0.012)	(0.012)

Autocorrelation estimates for z and $|z|$ are also given in Table I, as tests of the independence implications of a correctly fitted model. All models have a small but statistically significant negative autocorrelation in intradaily/overnight normalized returns—a result reflecting a small negative autocorrelation in the original log-differenced futures prices. At the daily horizon, the autocorrelation in normalized returns is smaller and not statistically significant. Autocorrelations in absolute normalized returns $|z|$ for intradaily/overnight data are reduced (although still statistically significant) under the multifactor Vjump2 and Vjump3 models, which indicates that the multifactor models capture intradaily volatility dynamics better. All models have a statistically significant −7% autocorrelation in daily $|z|$, which suggests the models are not fully capturing daily volatility dynamics.

II. Realized Variance

Define

$$RV_n = \sum_{m=1}^{M_n} \left[\ln\left(F_{n,m}\right) - \ln\left(F_{n,m-1}\right)\right]^2 \tag{14}$$

as the daily realized variance on day n from $M_n \leq 26$ sequential intradaily time intervals that begin 15 minutes after pit trading in the S&P 500 futures contract opens and typically have a duration of about 15 minutes. The realized variance literature relies heavily on the asymptotic convergence of realized variance to quadratic variation as the sampling frequency increases:

$$QV_n \equiv \int_{s=t}^{t+\tau_n^{daily}} (df_s)^2 = \int_{s=t}^{t+\tau_n^{daily}} \left(\sum_{i=1}^{I} V_{is} ds + \sum_{j=1-K}^{J} \gamma_j^2 dN_{js}\right). \tag{15}$$

The correlation between realized variance and quadratic variation in simulated Vjump3 data is 95% at the 15-minute horizon, and rises to 98% and 99.7% at five- and one-minute horizons, respectively. Because quadratic variation is an affine latent characteristic in affine models, with an analytical conditional characteristic function that is given in Appendix A, examining distributional properties of realized variance as a proxy for those of quadratic variation is another potentially useful diagnostic of the proposed time-series models.

The effective length of the intradaily trading period varies on a daily basis, making it desirable to rescale realized variance by the aggregate intradaily time interval

$$252\tau_n^{daily} = \sum_{m=1}^{M_n} 252\tau_{nm} = f_{daily} \exp\left(\boldsymbol{\beta}_{ID}{}' \boldsymbol{d}_n^{ID}\right), \tag{16}$$

where $\exp(\boldsymbol{\beta}_{ID}{}' \boldsymbol{d}_n^{ID})$ are the intradaily day-of-the-week effects graphed in Figure 1, and 252 converts the time units from yearly to daily. In particular,

$$Rvol_n = \sqrt{\frac{RV_n}{252\tau_n^{daily}}} \tag{17}$$

is the realized volatility on a daily (24-hour) Wednesday equivalent basis that can be compared to conditional or unconditional volatility assessments from daily close-to-close returns. The major impact of the daily rescaling is to eliminate the impact of half-days adjacent to holidays, which otherwise look like inliers.

Table II describes characteristics of various transforms of realized volatility, while Figure 8 graphs realized variance and volatility. Realized variance is an extremely skewed and leptokurtic random variable, with especially pronounced outliers during October 19 to 22, 1987. By contrast, a log transform for volatility (or variance) appears substantially better behaved, with substantially less

Table II

Summary Statistics for Daily Realized Volatility Measures

This table presents summary statistics for transforms of realized volatility $Rvol_n = \sqrt{\frac{\sum(\Delta \ln F)^2}{252\tau_n}}$, where $252\tau_n$ is the estimated length of the intradaily period in days, with an average value of 0.774 (Vjump1b estimates). ARMA models are estimated in RATS, using the Bayes information criterion for model selection. Major $Rvol_n$ outliers: 26.9% (10/20/1987), 14.8% (10/19/1987), 11.4% (10/22/1987), and 8.7% (10/10/2008).

	$Rvol_n^2$	$Rvol_n$	$\ln(Rvol_n)$
Maximum	0.027530	26.93%	−1.312
Minimum	0.000003	0.17%	−6.380
Mean	0.000130	0.91%	−4.825
(Std. error)	(0.000012)	(0.01%)	(0.006)
Median	0.000062	0.79%	−4.847
Std. deviation	0.000982	0.68%	0.477
Skewness	63.4	12.5	0.63
Excess kurtosis	4553	367	1.83
ARMA model	ARMA(3,1)	ARMA(3,1)	ARMA(3,2)

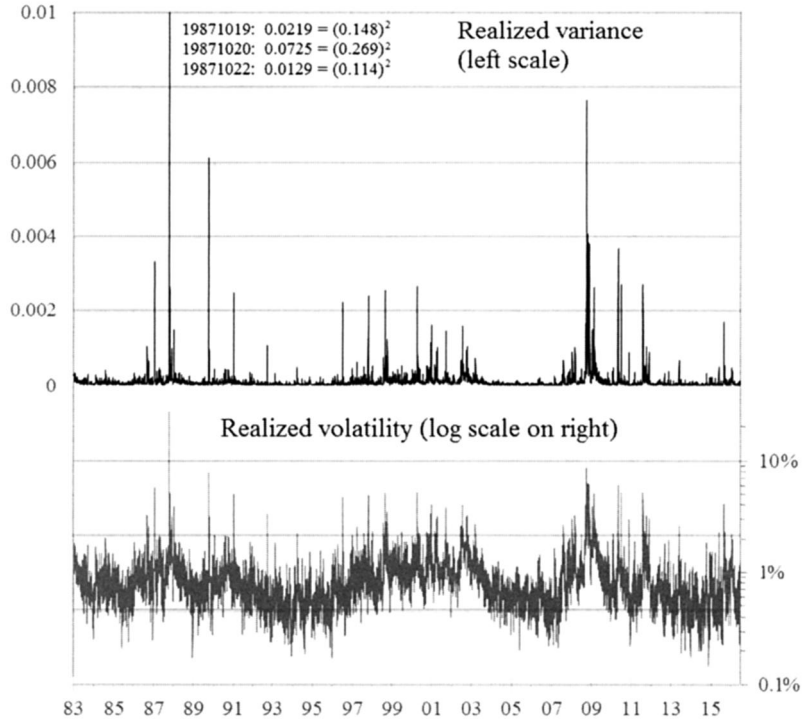

Figure 8. Daily realized variance (regular scale) and volatility (log scale).

pronounced skewness and excess kurtosis in Table II and more discernable persistence in Figure 8. Indeed, Figure 8 appears to offer significant support for the two-factor diffusive log variance process estimated on daily data by Chernov et al. (2003), in contrast to the affine specifications explored here. However, as discussed in Appendix A.3, this paper's extended Duffie, Pan, and Singleton (2000) volatility jump model implies a heavy-tailed distribution for quadratic variation that is potentially compatible with the occasional extreme outliers in realized variance.

A Box-Jenkins analysis indicates that realized variance follows an ARMA(3,1) process, using a Bayes information criterion for model selection. The statistical reliability of the least squares ARMA estimation methodology is questionable given the extreme nonnormality of realized variance data. Nevertheless, the result is qualitatively consistent with the Vjump3 model, which implies an ARMA(3, 3) process for quadratic variation.

Table III compares the models' ability to forecast realized variance with two other methodologies: ARMA forecasts of average intradaily realized variances at 1-, 5-, and 21-business-day horizons, and VIX-based forecasts of average realized variance (including overnight) over 21 business days. For the 1983 to 2008 period used in the original estimations, all Vjump models outperform ARMA-based forecasts, and the more general models do better. All forecasts fit poorly, because of extreme realized variances observed during the 1987 crash.

All forecasts perform comparably at a one-day horizon over the quieter 1990 to 2008 period that excludes the 1987 crash. The Vjump3 outperforms the simpler models at 5- and 21-day horizons. Unsurprisingly, the VIX-based forecasting methodology outforecasts all of the Vjump models at the 21-day horizon, given options markets have access to more information than forecasts based on past returns. All models have similar forecasting accuracy at one- and five-day horizons out-of-sample over the 2009 to 2016 period. The Vjump3 model of volatility dynamics outperforms the simpler models at the 21-day horizon, and comes close to matching the VIX-based forecasts.

Finally, how well the proposed models match the overall conditional distributions of realized variance realizations can in principle be evaluated via normal probability plots, in the same fashion used in Figure 7 above for intradaily/overnight and daily returns. Normalized residuals $z_{n+1}^{RV} = N^{-1}[\mathrm{CDF}^{QV}(RV_{n+1}|\boldsymbol{Y}_{n,M_n}, \hat{\Theta})]$ are computed by Fourier inversion, using the conditional characteristic function of quadratic variation in Appendix A.

It turns out, however, that conditional distributions of realized variances can differ substantially from those of quadratic variation. Whereas the correlation between 15-minute realized variance and quadratic variation is 95% for data simulated from the Vjump3 model, the correlation of the corresponding z-values is only 80%. (The z correlations on simulated Vjump3 data rise to 92% and 98% for five- and one-minute realized variances, respectively.) Consequently, the graphs in Figure 9 use simulation-based bias corrections and confidence intervals to compare what should be observed for ordered z_{n+1}^{RV} values with what

Table III

Forecasts of Average Daily Realized Variances over 1983 to 2016

This table presents the fit of various forecasts of future realized variances, which are measured in squared percentages. An average intradaily realized variance of 1.31 over 1983 to 2008 corresponds to a 1.14% realized volatility, scaled as in Table II to a daily horizon. VIX-based forecasts of average realized variances over 21 business days use the regression

$$252\,\overline{RV}_{t+1\to t+21} = \underset{}{-0.08} - \underset{(0.49)}{0.19}\,VIX_t + \underset{(0.77)}{0.89}\,VIX_t^2 \qquad (0.30)$$

on daily data over 1990 to 2008. Standard errors for the above regression are in parentheses, corrected for heteroscedasticity and for serial correlation from overlapping forecasts.

	Intradaily Realized Variance (Scaled)			Intradaily/ Overnight
	One-Day	Five-Day	21-Day	21-Day RV
1983–2008 (in-sample): Avg(RV) = 1.31 intradaily, 1.43 intradaily and overnight				
SD(RV):	9.83	6.06	3.62	4.73
R^2				
ARMA(3,1)	0.132	0.087	0.063	
Vjump1b	0.139	0.128	0.094	0.101
Vjump2	0.161	0.099	0.099	0.120
Vjump3	0.270	0.174	0.132	0.137
1990–2008 (in-sample): Avg(RV) = 1.18 intradaily, 1.26 intradaily/overnight				
SD(RV):	2.69	2.23	1.97	2.17
R^2				
ARMA(3,1)	0.440	0.421	0.288	
Vjump1b	0.535	0.585	0.350	0.327
Vjump2	0.517	0.521	0.366	0.342
Vjump3	0.503	0.610	0.440	0.419
VIX-based				0.537
2009–16 (out-of-sample): Avg(RV) = 0.94 intradaily, 1.17 intradaily/overnight				
SD(RV):	1.90	1.37	1.09	1.32
R^2				
ARMA(3,1)	0.280	0.345	0.317	
Vjump1b	0.351	0.445	0.319	0.333
Vjump2	0.360	0.501	0.436	0.454
Vjump3	0.314	0.447	0.475	0.537
VIX-based				0.569

is actually observed. In Table IV, I use similar simulation-based benchmarks to examine the moments and other characteristics of the z_{n+1}^{RV} values.

Two results stand out. First, the more general models match the conditional distributions better, using simulation-based benchmarks that correct the biases of CDFs based on quadratic variation. The Vjump2 model substantially reduces the frequency of realized variance inliers and outliers relative to the Vjump1b model. The Vjump3 model captures outliers even better than the

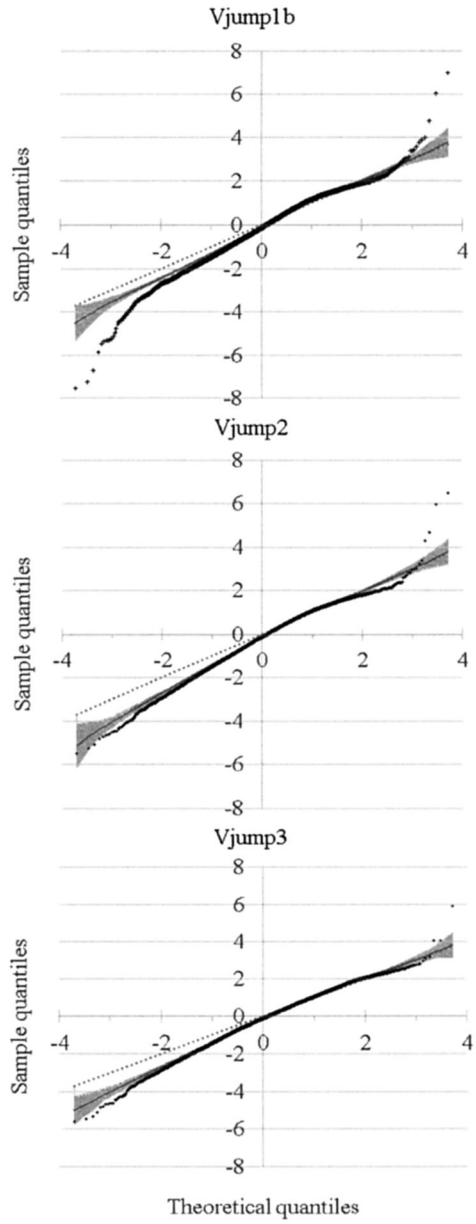

Figure 9. Normal probability plots for intradaily realized variance. The panels compare the ordered normalized residual values $z_{n+1}^{RV} = N^{-1}[\text{CDF}^{QV}(RV_{n+1}|\boldsymbol{Y}_{n,M_n}, \hat{\Theta})]$ (+ symbols on the vertical axis) with predicted values (dotted lines) based on quadratic variation's conditional CDFs and with average values (solid lines) from 100 runs of simulated data. The grey shaded areas are 95% confidence intervals for the deviation between observed data and average simulated values. (Color figure can be viewed at wileyonlinelibrary.com)

Table IV

Summary Statistics for the Normalized Residuals of Realized Variances over 1983 to 2008, on Actual and Simulated Data

This table presents statistics for the normalized residuals $z_{n+1}^{RV} = N^{-1}[CDF^{QV}(RV_{n+1}|Y_{n,M_n}, \hat{\Theta})]$, which should be i.i.d. standard Gaussian conditional on correct specification and on 15-minute realized variance closely approximating quadratic variation. Comparison of actual versus simulated summary statistics corrects for biases from a poor approximation. Simulated data are from 100 runs of 6,557 days each, using model-specific parameter estimates and time gaps. The t-statistics for compatibility between actual and simulated statistics are $[M^{act} - \text{Avg}(M^{sim})]/[\text{SD}(M^{sim})\sqrt{1.01}]$.

		Simulated Data		
Statistic	Actual Data	Average	Std. Deviation	t-Statistic
Vjump1b				
Maximum	>7[a]	3.80	0.34	9.41
Minimum	−7.55	−4.52	0.42	−7.17
Mean	−0.191	−0.106	0.012	−7.27
Median	−0.155	−0.093	0.017	−3.59
SD	1.265	1.158	0.011	9.99
Skewness	−.32	−.12	0.03	−8.17
Excess kurtosis	0.55	−.28	0.05	16.40
Vjump2				
Maximum	6.46	3.80	0.31	8.52
Minimum	−5.50	−5.13	0.52	−0.71
Mean	−0.225	−0.163	0.014	−4.35
Median	−0.121	−0.096	0.022	−1.16
SD	1.250	1.211	0.009	4.10
Skewness	−0.40	−0.28	0.03	−3.50
Excess kurtosis	0.16	−0.13	0.06	4.41
Vjump3				
Maximum	5.88	3.80	0.34	6.04
Minimum	−5.62	−5.01	0.40	−1.53
Mean	−0.190	−0.156	0.012	−2.77
Median	−0.119	−0.112	0.017	−0.39
SD	1.245	1.215	0.011	2.88
Skewness	−0.33	−0.20	0.03	−3.78
Excess kurtosis	0.20	−0.10	0.07	4.53

[a]The normalized residual observed on October 20, 1987 could not be computed for the Vjump1b model, but is in excess of 7. The summary statistics use a value of 7 for that observation.

Vjump2 model, but does slightly worse with regard to inliers. In all cases, however, the realized variance realization of $(26.9\%)^2$ on October 20, 1987 remains a major positive outlier.

Second, even the most general Vjump3 model has substantial and statistically significant deviations from simulation benchmarks, in both Table IV and Figure 9. While these affine models capture the conditional distributions of daily returns reasonably well, as indicated in Figure 6, there appears to be significant room for improvement in their predictions for the overall conditional distributions of realized variances—especially the frequency of realized variance inliers. However, the Vjump3 model does a reasonably good

job of capturing median, above median, and extreme realizations of realized variance.

III. Option Pricing Implications

A final criterion of the various models is how well they fit observed option prices. The diagnostics below use implicit volatilities from daily end-of-day settlement prices of American options on S&P 500 futures over January 1990 to June 2016. Because this paper focuses on high-frequency properties of stock index returns, I use the shortest maturity available, down to at least one full day before expiration. One-day serial option prices are typically from the Thursday settlement prior to expiration at Friday's close, while one-day quarterly option prices are typically from the Wednesday settlement prior to Friday's Special Opening Quotation. Maturities exceeding one month are not examined, because Bates (2012, Table 8) argues that longer term volatility dynamics not modeled in this paper become important at those horizons.

Similar to Andersen, Fusari, and Todorov (2015), I construct representative prices and associated implicit volatilities for strike prices X_{it} that are integer multiples of the at-the-money implicit volatility,

$$d_{it} \equiv \frac{\ln(X_{it}/F_t)}{IV_t^{atm}\sqrt{T_t}} = 0, \pm 1, \pm 2, \ldots, \tag{18}$$

where F_t is the futures settlement price and T_t is the option maturity, estimated using the Vjump1b time horizon parameters graphed in Figures 1 and 2. Because of much greater depth in puts than calls, out-of-the-money put prices are interpolated over zero to six standard deviations ($d = \{-6, \ldots, 0\}$), while call prices are interpolated over zero to two standard deviations ($d = \{0, 1, 2\}$), using the constrained cubic spline interpolation methodology of Bates (1991, 2000).

Any pricing kernel that is affine in the underlying risks implies an affine risk-neutral process that can be used to price European options on futures. This paper uses the following parsimonious pricing kernel discussed in Bates (2006, pp. 944–945):

$$d\ln \mathcal{M}_t = \mu_m\, dt - R\, d\ln F_t + \boldsymbol{R}_V' d\boldsymbol{V}_t, \tag{19}$$

where the risk premium parameters $\boldsymbol{rp} \equiv (R, \boldsymbol{R}_V)$ determine the compensations for equity, volatility, and jump risks. I examine three different parameterizations of $\boldsymbol{rp}$:

(i) rp1: the $(R, \boldsymbol{R}_V) = (2.45, \mathbf{0})$ parameters from Bates (2012), based on the estimated sensitivity over 1926 to 2006 of the daily conditional equity premium to $\boldsymbol{V}_t$;
(ii) rp2: $(R, \boldsymbol{R}_V) > \mathbf{0}$, using the best fits to option prices over 1990 to 2008; and
(iii) rp3: unconstrained $(R, \boldsymbol{R}_V)$, again using the best fits to option prices.

As discussed in Appendix C, the risk premia alter the intensity and average jump sizes of the underlying exponential and Gaussian jumps. The first two specifications imply more frequent and larger negative jumps in log futures prices under the risk-neutral measure than under the objective measure. The risk premia also affect the conditional equity premium of futures returns.

This paper uses option pricing fit as an additional diagnostic of the merits of the underlying time-series models. Consequently, options are priced *conditional* on the time-series parameter estimates and the filtered end-of-day conditional distributions $\hat{g}_{t|t}$ of $\boldsymbol{V}_t$. I evaluate fit using the loss function

$$\text{RMSE}\ (\boldsymbol{rp}) = \sqrt{\frac{1}{NOBS}\sum_{t,i}\left[\frac{\hat{o}\left(F_t, T_t, X_{it}, r_t|\hat{g}_{t|t}, \boldsymbol{rp}\right) - o^B(F_t, T_t, X_{it}, r_t, IV_{it})}{o^B_{IV}\left(F_t, T_t, X_{it}, r_t, IV_{it}\right)}\right]^2}, \quad (20)$$

where $\hat{o}(\cdot)$ is the model-specific European put or call option price estimate given the inputs,[22] $o^B_{it}(\cdot)$ is the corresponding Black (1976) European futures option price given implicit volatility IV_{it} from interpolated American option prices, and $o^B_{IV}(\cdot)$ is the corresponding option vega. The loss function uses the Broadie, Chernov, and Johannes (2007) approach of extrapolating from American to European futures option prices, while the inverse vega weights make the loss function approximately the root mean squared error of estimated versus observed implicit volatilities.

Estimates of $\boldsymbol{rp} = (R, \boldsymbol{R}_V)$ for the rp2 and rp3 specifications are based on minimizing equation (20) for standardized option prices over 1990 to 2008, with 2009 to 2016 used for out-of-sample diagnostics. Three additional criteria are used to assess the resulting fits:

(i) the *level* of the volatility smirk, as measured by IV_t^{atm};
(ii) the *slope* of the volatility smirk, as measured by the divergence $SKEW_t \equiv IV_t^{call} - IV_t^{put}$ between implicit volatilities of calls and puts that are one standard deviation out-of-the-money; and
(iii) the log likelihood implications over 1983 to 2016 of the ***rp*** estimates for conditional intradaily/overnight equity premia.

The second criterion is the Bates (1991, 1997) skewness premium measure of asymmetry in risk-neutral distributions, expressed in implicit volatility terms. Backus et al.'s (1997) Gram-Charlier approximation indicates that implicit volatilities from options that are one standard deviation out-of-the-money are linearly sensitive to skewness but insensitive to excess kurtosis, making this divergence roughly proportional to risk-neutral skewness.[23]

Results from the various time-series models and ***rp*** specifications are reported in Table V. Overall, more state variables (Vjump1b, ..., Vjump3)

[22] See Bates (2012), equation (50).

[23] Bakshi, Kapadia, and Madan (2003) provide a more accurate method of estimating risk-neutral skewness from option prices. However, their approach requires a greater strike price range for calls than is reliably available over 1990 to 2008, whereas calls one standard deviation out-of-the-money are almost always actively traded.

Table V

Option and Time-Series Fit from Various Specifications of Risk Premia

This table presents how well the models fit option prices and returns using three estimates of risk premia: $(R;\ \boldsymbol{R}_V) = (2.45;\ \mathbf{0})$ (rp1), $(R;\ \boldsymbol{R}_V) > \mathbf{0}$ (rp2), and unconstrained $(R;\ \boldsymbol{R}_V)$ (rp3). *IV-RMSE* is the overall fit to all short-maturity options' implicit volatilities over 1990 to 2016. $\Delta \ln L \mid \{\hat{g}_{t|t}\}$ is the change in log likelihoods of intradaily and overnight returns over 1983 to 2016 from the resulting changes in the conditional equity premium, with filtered $\hat{g}_{t|t}$ unchanged. $\widehat{IV}^{atm}$ is the predicted at-the-money implicit volatility. $\widehat{SKEW} = \widehat{IV}^{call} - \widehat{IV}^{put}$ is the predicted slope of the volatility smirk, using calls and puts that are one standard deviation out-of-the-money.

	Overall *IV-RMSE*, in %				Time series: $\Delta \ln L \mid \{\hat{g}_{t|t}\}$		
	rp1	rp2	rp3		rp1	rp2	rp3
Vjump1b	4.41	4.37	4.32		5.49	1.58	−1,484
Vjump2	4.49	4.00	3.93		5.50	6.76	−26,533
Vjump3	4.00	3.79	3.63		−10.41	−12.00	−7,814
		Avg($\widehat{IV}^{atm}$)		data		RMSE($\widehat{IV}^{atm}$)	
Vjump1b	17.15	17.48	17.38	17.06	4.05	4.03	4.02
Vjump2	15.86	16.75	16.68	17.06	4.09	3.75	3.81
Vjump3	15.52	16.78	16.83	17.06	3.73	3.29	3.28
		Avg($\widehat{SKEW}$)		data		RMSE($\widehat{SKEW}$)	
Vjump1b	−1.86	−1.91	−2.03	−3.97	2.72	2.72	2.61
Vjump2	−2.11	−2.27	−2.60	−3.97	2.37	2.31	2.06
Vjump3	−2.16	−1.90	−2.37	−3.97	2.24	2.54	2.18

generally lead to more accurate option prices, with further increases in accuracy when the $(R, \boldsymbol{R}_V)$ parameters are allowed greater flexibility. Overall RMSE drops from 4.41% under the Vjump1b + rp1 specification to 3.63% under the Vjump3 + rp3 specifications.[24] The $(R, \boldsymbol{R}_V)$ parameters for rp3 that best fit option prices yield highly implausible conditional equity premia over 1983 to 2016, whereas the constrained rp1 and rp2 specifications appear innocuous. The implications for risk-neutral parameters are given in Table C.I in Appendix C.

Much of the improvement in fit of Vjump3 versus Vjump1b appears attributable to more accurate prediction of the overall level of implicit volatility, as proxied by IV_t^{atm}. This parallels the results in Table II that the Vjump3 model forecasts future realized variance more accurately at longer horizons than the Vjump2 or Vjump1b models, and approaches the accuracy of the VIX-based forecasts. The Vjump2 model generates the steepest and most accurate predictions of the slope of the volatility smirk.

[24] Andersen, Fusari, and Todorov (2015) achieve an overall RMSE of 1.40% across all maturities over 1996 to 2010 for their best-fitting three-factor model. However, they use the Bates (1996, 2000) approach of estimating the risk-neutral parameters and implicit state variables that best match observed option prices, with a penalty if the total daily implicit diffusive variance common to both objective and risk-neutral measures diverges excessively from an intradaily nonparametric estimate. By contrast, I estimate parameters and state variables from past intradaily and overnight futures returns, with only a few additional ***rp*** parameters used to match option prices.

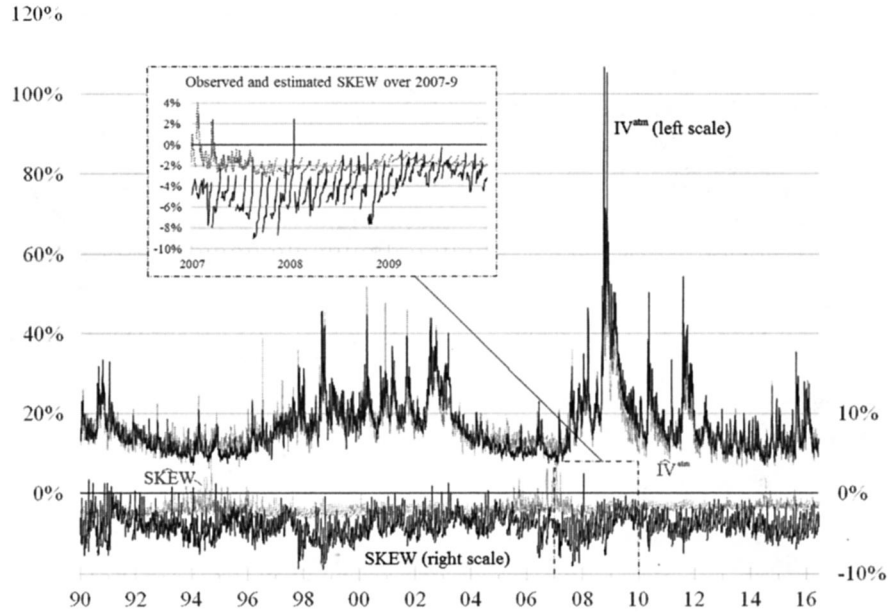

Figure 10. Observed and estimated at-the-money implicit volatilities IV^{atm}, and divergences $SKEW = IV^{call} - IV^{put}$ for calls and puts one standard deviation out-of-the-money. Option maturities are the shortest available with at least one day to maturity. Line breaks in the observed and estimated SKEW series indicate option maturity shifts from one day to one month. (Color figure can be viewed at wileyonlinelibrary.com)

There is a strong maturity effect on the slope of the volatility smirk that all models largely fail to capture. The volatility smirk measured by SKEW typically flattens as options approach maturity. And while the Vjump3/rp2 estimates graphed in Figure 10 are not far off at the one-day horizon, the estimates do increasingly poorly at longer five- or 18-day horizons. Even the most flexible risk-neutral parameterizations under the rp3 specification generally fail to match this maturity effect, as shown in Table VI.

In sum, the time-series models fit observed option prices progressively better as more state variables are added, with Vjump3 achieving the best overall fit. However, there remains a substantial and systematic gap between predicted and observed volatility smirks of less than one month's maturity. Possible explanations include greater downside jump risk, more aggressive leverage and volatility feedback effects than those in the models, or greater aversion to downside risk than is captured by the pricing kernel specification (19).

The first explanation seems unlikely. Jump-diffusive option pricing models with independent returns such as Bates (1991) or Andersen, Fusari, and Todorov (2017) counterfactually predict that the volatility smirk should steepen rather than flatten as options approach maturity. The third explanation is proposed by Andersen, Fusari, and Todorov (2015) in the form of an additional U-factor inferred from movements in risk-neutral left tail risk that is orthogonal to movements in diffusive variance.

Table VI
Average $\widehat{SKEW}$ by Maturity (in Business Days)

This table presents average estimated $\widehat{SKEW} = \widehat{IV}^{call} - \widehat{IV}^{put}$ and corresponding observed values for the specified maturities, based on 311 to 316 monthly observations over 1990 to 2016.

	Vjump1b			Vjump2			Vjump3			
	rp1	rp2	rp3	rp1	rp2	rp3	rp1	rp2	rp3	data
One-day	−1.25	−1.30	−1.34	−1.32	−1.41	−1.72	−1.22	−1.32	−1.76	−2.46
Five-day	−1.95	−2.01	−2.11	−2.08	−2.26	−2.59	−1.92	−1.81	−2.31	−3.46
18-day	−1.83	−1.87	−2.01	−2.19	−2.33	−2.66	−2.45	−2.02	−2.45	−4.70

Overall, however, I feel that exploring alternative models of leverage and volatility feedback effects is the most promising area for future research. As Das and Sundaram (1999) discuss, a direct relationship between volatility smirks and option maturity at short maturities is suggestive of substantial distributional randomization, such as from stochastic volatility plus leverage. The time-series model in equations (1) to (3) is based on Duffie, Pan, and Singleton (2000) because it is the earliest and most tractable volatility jump model. But other time-series models even within an affine framework (e.g., Andersen, Fusari, and Todorov (2015)), as well as nonaffine models, might be more compatible with short-maturity option prices.

IV. Summary

Finite-activity jump-diffusion models such as Merton (1976) posit that log-differenced asset prices are drawn from a mixture of distributions, with major daily outliers the outcome of a draw from a higher volatility distribution. This model can be viewed as positing instantaneous but instantaneously transitory spikes in intradaily and daily volatility. The intradaily evidence does not support this description of volatility evolution. Instead, large daily market movements are the accumulation over the day of a series of rapid and self-exciting intradaily increases in conditional volatility, typically accompanied by a falling market. Volatility can accelerate rapidly from relatively low levels and can subside quickly from high levels, but the shifts take time to develop within a given day and can spill over into subsequent days. These short-lived volatility spikes affect both diffusive and jump volatility, with the former more important. The initiation of a volatility spike is more likely when core volatility is already high.

The central intradaily dynamic proposed and estimated in this paper consists of self-exciting intradaily volatility spikes that accompany modest and predominantly negative intradaily stock market jumps. The results are largely consistent with the evidence from the nonparametric realized variance literature that intradaily price jumps tend to be small, with the largest ones in the Vjump3 model having a standard deviation of 1%. Their importance lies more in their dynamic implications: a signal that there is immediate risk of more

price/volatility cojumps and of a run of such jumps that could accumulate into a major daily price movement. Runs of successive intradaily price/volatility cojumps generated market moves exceeding 10% in magnitude in 1987 and 2008.

Initial submission: February 9, 2016; Accepted: November 10, 2017
Editors: Bruno Biais, Michael R. Roberts, and Kenneth J. Singleton

Appendix A: Joint Characteristic Functions

A.1. Models with One Underlying State Variable

The fundamental building blocks for the multifactor and multijump models in this paper are based on the single-factor Duffie, Pan, and Singleton (2000) model, which has constant-intensity synchronous correlated jumps in the log futures prices f_t and underlying spot variance V_t. Let x_t be some additional latent variable of interest: the accumulated number or size of jumps, or quadratic variation and its integrated variance and squared jump components. Each of these variables follows a pure jump process, which implies that $(f_t,\ V_t,\ x_t)$ evolve as

$$\begin{aligned} df_t &= \left[\mu_0 + (\mu_1 - 1/2)\, V_t\right]dt + \sqrt{V_t}dW_t + \left(\gamma dN_t - \lambda \bar{k} dt\right), \\ dV_t &= (\alpha - \beta V_t)\ dt + \sigma\sqrt{V_t}dW_{Vt} + \gamma_V dN_t, \\ dx_t &= \mu_x\ V_t dt + \gamma_x dN_t, \end{aligned} \tag{A.1}$$

where W_t and W_{Vt} are Wiener processes with correlation ρ, N_t is a Poisson counter with constant intensity λ, $\gamma_V \sim \text{Exp}(\bar{\gamma}_V)$ is the exponentially distributed jump in spot variance conditional on a jump, and $\gamma = \rho_J\ \gamma_V + \gamma_f$ for $\gamma_f \sim N(\bar{\gamma}_f, \delta_f^2)$ is the correlated jump in log futures prices, with expected percentage jump size $\bar{k} = \text{E}(e^{\gamma_J}) = e^{\bar{\gamma}_f + 1/2\delta_f^2}/(1 - \rho_J\bar{\gamma}_V) - 1$. Specific processes for x_t are discussed below.

The generalized Fourier transform for future $\boldsymbol{z}_{t+\tau} = (f_{t+\tau}, V_{t+\tau},\ x_{t+\tau})$ and complex $(\Phi,\ \boldsymbol{\psi},\ \boldsymbol{\xi})$ conditional on current $\boldsymbol{z}_t$ is

$$\begin{aligned} &\mathcal{F}(\tau; \Phi, \boldsymbol{\psi}, \boldsymbol{\xi} | \boldsymbol{z}_t) \equiv \text{E}\left[\exp\left(\Phi f_{t+\tau} + \boldsymbol{\psi} V_{t+\tau} + \boldsymbol{\xi} x_{t+\tau}\right) \mid \boldsymbol{z}_t\right] \\ &= \exp\left[\Phi f_t + \boldsymbol{\xi} x_t + C(\tau; \Phi, \boldsymbol{\psi}, \boldsymbol{\xi}) \right. \\ &\quad \left. + D(\tau; \Phi, \boldsymbol{\psi}, \boldsymbol{\xi}) V_t + \lambda E(\tau; \Phi, \boldsymbol{\psi}, \boldsymbol{\xi})\right]. \end{aligned} \tag{A.2}$$

The function $\mathcal{F}(\cdot)$ solves the backward Kolmogorov equation $E_t d\mathcal{F}(\cdot) = 0$ associated with (A.1), implying that $C(\tau;\ \cdot)$, $D(\tau;\ \cdot)$, and $E(\tau;\ \cdot)$ solve the following system of ordinary differential equations subject to $C\ (0;\ \cdot) =\ E\ (0;\ \cdot) =\ 0$ and

$D(0;\,\cdot) = \psi$:

$$\begin{aligned} C_\tau &= \mu_0\,\Phi + \alpha D \\ D_\tau &= N(\Phi,\xi) + M(\Phi)\,D + {}^1\!/_2\sigma^2 D^2 \\ E_\tau &= \mathrm{E}\left[e^{\Phi(\gamma_f+\rho_J\gamma_V)+D(\tau;\cdot)\gamma_V+\xi\gamma_x}\right] - 1 - \Phi\bar{k}, \end{aligned} \tag{A.3}$$

where $N(\Phi,\xi) = {}^1\!/_2\Phi^2 + \left(\mu_1 - {}^1\!/_2\right)\Phi + \mu_x\xi$ and $M(\Phi) = \rho\sigma\Phi - \beta$. I use ξ when estimating the latent characteristic $x_{t+\tau} - x_t$, and otherwise set it to zero. The solution for $D(\tau;\,\cdot)$ is[25]

$$D\,(\tau;\Phi,\psi,\xi) = \frac{2N(\Phi,\xi) + \psi\left[M(\Phi) + R(\tau,\Phi,\xi)\right]}{R(\tau,\Phi,\xi) - M(\Phi) - \sigma^2\psi}\,, \tag{A.4}$$

where

$$R\,(\tau,\Phi,\xi) = \gamma\,(\Phi,\xi)\,\frac{e^{\gamma(\Phi,\,\xi)\tau}+1}{e^{\gamma(\Phi,\,\xi)\tau}-1} \text{ and}$$

$$\gamma\,(\Phi,\xi) = \sqrt{M(\Phi)^2 - 2\sigma^2 N(\Phi,\xi)}\,. \tag{A.5}$$

The solution for $C(\tau;\,\cdot)$ is

$$\begin{aligned} C\,(\tau;\Phi,\psi,\xi) = \mu_0\Phi\tau &- \frac{\alpha\tau}{\sigma^2}\left[M(\Phi) - \gamma\,(\Phi,\xi)\right] \\ &- \frac{2\alpha}{\sigma^2}\ln\left\{1 + \left[M(\Phi) - \gamma\,(\Phi,\xi)\right]\frac{1 - e^{\gamma(\Phi,\xi)\tau}}{2\gamma\,(\Phi,\xi)}\right\} \\ &- \frac{2\alpha}{\sigma^2}\ln\left[1 - \frac{\sigma^2\psi}{R(\tau,\Phi,\xi) - M(\Phi)}\right]. \end{aligned} \tag{A.6}$$

The solution for $E(\tau;\,\cdot)$ depends on the specification of the jump distribution γ_x of x_t. For the benchmark model with $\xi = 0$ that is used when filtering and estimating models,

$$\begin{aligned} E\,(\tau;\Phi,\psi,\,0) &= e^{\Phi\bar{\gamma}_f + {}^1\!/_2\Phi^2\delta_f^2}\left\{\frac{b}{d}\tau - e\ln\left[1 + \frac{c\left(e^{-\gamma(\Phi,0)\tau} - 1\right)}{c+d}\right]\right\} - \left(1 + \Phi\bar{k}\right)\tau \\ &\equiv H(\tau;\Phi,\psi) - \left(1 + \Phi\bar{k}\right)\tau, \end{aligned} \tag{A.7}$$

where

$$b = \left[M(\Phi) - \gamma\,(\Phi,0)\right] + \sigma^2\psi,$$

$$c = \left\{-s\left[M(\Phi) + \gamma\,(\Phi,0)\right] - 2\bar{\gamma}_V N(\Phi,0)\right\} + \psi\left\{-s\sigma^2 - \bar{\gamma}_V\left[M(\Phi) - \gamma\,(\Phi,0)\right]\right\},$$

[25] If jumps have stochastic intensity $\lambda_t = \lambda + \lambda_1 V_t$, then $D(\tau;\,\cdot)$ solves $D_\tau = N + MD + {}^1\!/_2\sigma^2 D^2 + \lambda_1 E_\tau(\tau;\Phi,D(\cdot),\xi)$. This is of cubic rather than quadratic order when $\xi = 0$, and has an implicit rather than explicit solution for $D(\tau;\,\cdot)$, precluding rapid evaluation. Such models typically are solved numerically. See, for example, Carr and Wu (2008).

$$d = \{s\left[M(\Phi) - \gamma(\Phi, 0)\right] + 2\bar{\gamma}_V N(\Phi, 0)\} + \psi\left\{s\sigma^2 + \bar{\gamma}_V\left[M(\Phi) + \gamma(\Phi, 0)\right]\right\},$$

$$e = \frac{2\bar{\gamma}_V}{2\bar{\gamma}_V^2 N(\Phi, 0) + 2\bar{\gamma}_V M(\Phi)s + \sigma^2 s^2}, \text{ and}$$

$$s = 1 - \rho_J \bar{\gamma}_V \Phi. \tag{A.8}$$

When x_t is the accumulated number or size of jumps, or the integrated variance, $E(\tau; \cdot)$ takes the following forms, for $H(\cdot)$ defined as in (A.7) above:

x_t	μ_x	γ_x	$E(\tau; \Phi, \psi, \xi)$
N_t	0	1	$e^{\xi} H(\tau; \Phi, \psi) - (1 + \Phi\bar{k})\tau$
$\int_0^t \gamma dN_s$	0	γ	$H(\tau; \Phi + \xi, \psi) - (1 + \Phi\bar{k})\tau$
$\int_0^t \gamma_V dN_s$	0	γ_V	$H(\tau; \Phi, \psi + \xi) - (1 + \Phi\bar{k})\tau$
$\int_0^t V_s ds$	1	0	$H(\tau; \Phi, \psi) - (1 + \Phi\bar{k})\tau$

For quadratic variation $x_t = \int_0^t (V_s ds + \gamma^2 dN_s)$, or its squared jump subcomponent, the jump size $\gamma_x = \gamma^2 = (\gamma_f + \rho_{sv}\gamma_V)^2$. This has a heavy-tailed distribution when γ_V is exponentially distributed, with infinite values for the moment generating function $\mathrm{E}[e^{\xi\gamma^2}]$ when ξ is real and positive. Quadratic variation is consequently also heavy-tailed for the Duffie, Pan, and Singleton (2000) process, although the conditional characteristic function and moments of all orders exist. Integrating successively over the independent Gaussian and exponential distributions of γ_f and γ_V, the generalized transform of the jump components is

$$\begin{aligned}
\mathcal{F}^J(\Phi, \psi, \xi) &\equiv \mathrm{E}\exp\left[\Phi\left(\gamma_f + \rho_{sv}\gamma_V\right) + \psi\gamma_V + \xi\left(\gamma_f + \rho_{sv}\gamma_V\right)^2\right] \\
&= \frac{\mathrm{E}\left\{\exp\left[a(\xi)\gamma_V^2 + b(\Phi, \psi, \xi)\gamma_V + c(\Phi, \xi)\right]\right\}}{\sqrt{1 - 2\delta_f^2\xi}} \\
&= \frac{e^{c(\Phi,\xi)}}{2\bar{\gamma}_V}\sqrt{\frac{-\pi}{\rho_{sv}^2\xi}}\, w\left(d(\xi)\frac{b(\Phi, \psi, \xi)\bar{\gamma}_V - 1}{2\bar{\gamma}_V\sqrt{a(\xi)}}\right),
\end{aligned} \tag{A.9}$$

where

$$\begin{aligned}
a(\xi) &= \frac{\rho_{sv}^2\xi}{1 - 2\delta_f^2\xi}, \\
b(\Phi, \psi, \xi) &= \psi + \frac{\rho_{sv}\left(\Phi + 2\bar{\gamma}_f\xi\right)}{1 - 2\delta_f^2\xi}, \\
c(\Phi, \xi) &= \frac{{}^1\!/_2\delta_f^2\Phi^2 + \bar{\gamma}_f\Phi + \bar{\gamma}_f^2\xi}{1 - 2\delta_f^2\xi}, \\
d(\xi) &= \mathrm{Sign}\left\{\mathrm{Im}\left[a(\xi)\right]\right\} = \pm 1,
\end{aligned} \tag{A.10}$$

and $w(\boldsymbol{z})$ for complex-valued $\boldsymbol{z}$ is the Fadeeva or plasma-dispersion function (equation 7.1.3 in Abramowitz and Stegun (1972, p.297)). It is a scaled version of the complex complementary error function ($w(\boldsymbol{z}) = e^{-\boldsymbol{z}^2}$ erfc$(-i\boldsymbol{z})$), and can be evaluated using algorithm 680 of Poppe and Wijers (1990).[26] Equation (A.9) is well defined for complex-valued $\boldsymbol{\xi}$ provided $Re[a(\boldsymbol{\xi})] < 0$—which is *not* true for small positive real values of ξ. The jump term $E(\tau; \Phi, \boldsymbol{\psi}, \boldsymbol{\xi})$ in (A.2) and (A.3) that is used for estimating latent quadratic variation or its squared jump component given parameter estimates can then be computed numerically:

$$E\ (\tau; \Phi, \boldsymbol{\psi}, \boldsymbol{\xi}) = \int_{s=0}^{\tau} \mathcal{F}^J\,(\Phi, D(s;\ \cdot), \boldsymbol{\xi})\ ds - \left(1 + \Phi \bar{k}\right) \tau. \tag{A.11}$$

I use nine-point trapezoidal integration to compute (A.11).

A.2. Multiple State Variables

Because all state variables V_{it} are assumed to evolve independently intraperiod, log characteristic functions are the sum of the log characteristic functions associated with each V_{it}. Define $\Theta_i^{diff} = (\mu_i, \alpha_i, \beta_i, \sigma_i, \rho_i; \mu_{xi})$ as the diffusive parameters associated with the variance process V_{it} and latent characteristic x_{it}, and define $\Theta_j^{jump} = (\bar{\gamma}_{Vj}, \rho_j, \bar{\gamma}_{\bar{f}j}, \delta_j)$ as the jump parameters associated with jump process N_{jt}. Define $C_i(\tau; \Phi, \boldsymbol{\psi}_i, \boldsymbol{\xi}_i)$ and $D_i(\tau; \Phi, \boldsymbol{\psi}_i, \boldsymbol{\xi}_i)$ as equations (A.6) and (A.4) evaluated at parameter values Θ_i^{diff}. For $i > 1$, $(\alpha_i, \sigma_i, \rho_i) = 0$ and $C_i = 0$. Define $E_j(\tau; \Phi, \boldsymbol{\psi}_j, \xi_j)$ for $j > 0$ as the relevant above expression for $E(\tau; \Phi, \boldsymbol{\psi}_j, \xi_j)$ evaluated at $(\Theta_j^{diff}, \Theta_i^{jump})$. Finally, let $E_0(\tau; \Phi, \xi_0)$ be the solution in the simpler special case associated with jump process N_{0t}, for futures jumps that are unaccompanied by volatility jumps. Because jump intensities are assumed constant intraperiod, the generalized Fourier transform for future $\boldsymbol{z}_{t+\tau} = (f_{t+\tau}, \boldsymbol{V}_{t+\tau}, \boldsymbol{x}_{t+\tau})$ conditional on current $\boldsymbol{z}_t$ is a multifactor extension of (A.2):

$$\begin{aligned}
\mathcal{F}(\tau; \Phi, \boldsymbol{\psi}, \boldsymbol{\xi} |\ \boldsymbol{z}_t) \ &\equiv\ \mathrm{E}\left[\exp\left(\Phi f_{t+\tau} + \boldsymbol{\psi}' \boldsymbol{V}_{t+\tau} + \boldsymbol{\xi}' \boldsymbol{x}_{t+\tau}\right) |\ \boldsymbol{z}_t\right] \\
&= \exp\Bigg[\Phi f_t + \mu_0 \Phi \tau + \boldsymbol{\xi}' \boldsymbol{x}_t + \sum_{i=1}^{I} \left[C_i\left(\tau; \Phi, \boldsymbol{\psi}_i, \boldsymbol{\xi}_i\right) + D_i\left(\tau; \Phi, \boldsymbol{\psi}_i, \boldsymbol{\xi}_i\right) V_{it}\right] \\
&\quad + \lambda_{01} V_{1t} E_0\left(\tau; \Phi, \xi_0\right) + \sum_{j=1}^{J} \left(\lambda_{j0} + \boldsymbol{\lambda}_j' \boldsymbol{V}_t\right) E_j\left(\tau; \Phi, \boldsymbol{\psi}_j, \boldsymbol{\xi}_j\right)\Bigg].
\end{aligned} \tag{A.12}$$

[26] Poppe and Wijers' (1990) algorithm is accurate to 14 significant digits, whereas the complex-valued Faddeva function ZERFE in IMSL is accurate to only 10 digits. Furthermore, ZERFE does not appear to be fully reliable for all values of ξ, when compared with direct numerical integration over the exponential density of γ_V.

A.3. Time Aggregation

The key modification in this paper's model relative to Duffie, Pan, and Singleton (2000) is to allow jump intensities to vary across periods, while maintaining the Duffie, Pan, and Singleton (2000) assumption of a constant intraperiod jump intensity. By iterating expectations over (A.12) progressively backwards in time, the multiperiod conditional cumulant-generating function takes the affine concatenated form

$$\ln \mathrm{E}\left[e^{\Phi(f_T - f_t) + \boldsymbol{\psi}' \boldsymbol{V}_T + \boldsymbol{\xi}'(\boldsymbol{x}_T - \boldsymbol{x}_t)} | \boldsymbol{V}_t\right]$$

$$= \mu_0 \, \Phi (T - t) + \sum_{i=1}^{I} C^i_{t,T}(\Phi, \boldsymbol{\psi}, \boldsymbol{\xi}) + D^i_{t,T}(\Phi, \boldsymbol{\psi}, \boldsymbol{\xi}) V_{it}. \tag{A.13}$$

Its components satisfy the backward recursion

$$\begin{aligned} D^1_{t,T} &= D_1\left(\tau_t; \Phi, D^1_{t+1,T}, \boldsymbol{\xi}_1\right) + \lambda_{01} E_0\left(\tau_t; \Phi, \boldsymbol{\xi}_0\right) + \sum_{j=1}^{J} \lambda_{j1} E_1\left(\tau_t; \Phi, D^1_{t+1,T}, \boldsymbol{\xi}_j\right), \\ D^i_{t,T} &= D_i\left(\tau_t; \Phi, D^i_{t+1,T}, \boldsymbol{\xi}_i\right) + \lambda_{ii} E_i\left(\tau_t; \Phi, D^i_{t+1,T}, \boldsymbol{\xi}_i\right) \text{ for } i > 1, \\ C^i_{t,T} &= C^i_{t+1,T} + C_i\left(\tau; \Phi, D^i_{t+1,T}, \boldsymbol{\xi}_i\right) + \lambda_{i0} E_i\left(\tau; \Phi, D^i_{t+1,T}, \boldsymbol{\xi}_i\right) \text{ for } i \geq 1, \end{aligned} \tag{A.14}$$

subject to the terminal condition $(C^i_{T,T},\ D^i_{T,T}) = (0,\ \boldsymbol{\psi}_i)$ for $i = 1, \ldots, I$. If overnight periods are omitted, as in the cumulant-generating function associated with N-day future intradaily quadratic variation, the relevant $\boldsymbol{\xi}_j$ values are set to zero on overnight periods within the recursion.

Appendix B: Estimates of the Log Futures Price Process

The tables below contain parameter estimates and log likelihoods for the log futures price process

$$df_t = \mu_0 \, dt + \sum_{i=1}^{I} \left[\left(\mu_i - {}^1\!/_2\right) V_{it} dt + \sqrt{V_{it}} dW_{it}\right] + \sum_{j=1-K}^{J} \gamma_j dN_{jt} - \lambda_{jt} \bar{k}_j dt,$$

$$dV_{1t} = (\alpha - \beta_1 V_{1t})\, dt + \sigma \sqrt{V_{1t}} dW_{Vt} + \gamma_{V1} dN_{1t},$$

$$dV_{it} = -\beta_i V_{it} dt + \gamma_{Vi} dN_{it} \text{ for } i > 1, \tag{B.1}$$

where I is the number of state variables in $\boldsymbol{V}_t$, J is the number of synchronous jumps in spot variance and futures prices, and K is the number of jumps in futures prices only. Diffusive shocks dW_{1t} and dW_{Vt} have correlation ρ. The intraperiod jump intensities λ_{jt} of Poisson counter N_{jt} and associated joint jump distributions of $(\gamma_j,\ \gamma_{Vj})$ are in Table B.IV below.

Table B.I
Log Likelihoods of Various Models

Model	I	J	K	Number of Parameters	$\ln L$	$\Delta \ln L$ 0–5 ticks	$\Delta \ln L$ >5 ticks	$\Delta \ln L$ All
In-sample SP futures (1983–2008)								
SVJ1	1	0	1	28	891,425.32			
Vjump1a	1	1	0	30	892,063.47	740.48	−102.32	638.16
Vjump1b	1	1	1	33	892,575.37	1,533.22	−1,021.32	511.90
Vjump2	2	2	1	42[a]	893,212.58	255.16	382.05	637.21
Vjump3	3	3	1	51	893,432.73	146.89	73.24	220.13
Vjump20	2	2	1	41[a]	892,940.09	−550.57[b]	286.08[b]	−264.49[b]
Vjump30	3	3	1	49[a]	893,211.30	−311.13[b]	89.71[b]	−221.42[b]
					$\ln L$	$\Delta \ln L$ 0–3 ticks	$\Delta \ln L$ >3 ticks	$\Delta \ln L$ All
Out-of-sample E-minis (2009–16)								
SVJ1					264,883.15			
Vjump1a					264,849.78	−80.79	47.48	−33.31
Vjump1b					265,044.26	660.18	−499.01	161.17
Vjump2					265,196.38	900.44	−587.14	313.30
Vjump3					265,261.23	1040.69	−662.55	378.14
Vjump20[b]					265,109.41	−313.42	226.44	−86.97
Vjump30[b]					265,160.85	−311.13	187.21	−100.38

[a]Multifactor models use the Vjump1b estimates of overnight/intradaily and diurnal seasonals.
[b]$\Delta \ln L$ for Vjump20 and Vjump30 is relative to the Vjump2 and Vjump3 fit, respectively.

Table B.II
Volatility-Dependent Changes in Log Likelihoods Relative to Nested Models

This table categorizes changes $\Delta \ln L$ in log likelihoods of nested models based on the previous day's realized volatility. The tercile breakpoints of 0.62% and 0.96% that determine low, medium, and high volatility are based on all intradaily realized volatilities over 1983 to 2016. The change in log likelihood for Vjump1a is relative to the SVJ1 model, while $\Delta \ln L$ for Vjump20 and Vjump30 is relative to the Vjump2 and Vjump3 fit, respectively.

	$\Delta \ln L$ in 1983–2008			$\Delta \ln L$ in 2009–2016		
RV_{n-1} tercile	Low	Medium	High	Low	Medium	High
Vjump1a	281.80	232.28	123.70	40.56	−30.63	−42.85
Vjump1b	246.14	145.60	120.68	120.55	51.88	22.30
Vjump2	161.31	148.80	326.61	84.16	12.90	55.33
Vjump3	67.53	78.58	73.52	40.01	23.11	1.95
Vjump20	−84.30	−0.99	−179.61	−101.95	5.58	8.51
Vjump30	−64.78	−44.14	−112.88	−79.05	−6.39	−16.18
% of sample	30%	38%	33%	46%	29%	25%

Table B.III

Parameter Estimates for Specific Models

This table presents estimates of parameters of the conditional mean and the variance processes in equation (B.1) above. Estimates are generally on an annualized basis, with Tuesday close to Wednesday close equal to 1/252 years. The half-lives $HL_i = 252(\ln 2)/(\beta_i - \lambda_{ii}\bar{\gamma}_{Vi})$ to variance shocks are reported in days. ρ^{adj} is the value of $\rho = \text{Corr}(dW_{1t}, dW_{Vt})$ if the jumps $(\gamma_0, \gamma_1, \gamma_{V1})$ are replaced with diffusive equivalents. Standard errors are in parentheses.

	Vjump1a	Vjump1b	Vjump2		Vjump3		
	V_{1t}	V_{1t}	V_{1t}	V_{2t}	V_{1t}	V_{2t}	V_{3t}
			Conditional mean				
μ_0	−0.10	−0.08	−0.08		0.01		
	(0.02)	(0.03)	(0.04)		(0.04)		
μ_i	8.0	8.0	5.9	7.4	2.5	1.9	0.3
	(1.5)	(2.5)	(4.3)	(2.9)	(9.0)	(11.7)	(3.7)
			Variance processes				
$\sqrt{\text{E}(V_i)}$	0.155	0.131	0.108	0.082	0.092	0.070	0.071
	(0.003)	(0.003)	(0.003)	(0.004)	(0.004)	(0.004)	(0.009)
HL_i (days)	3.6	5.2	9.4	0.35	13.4	0.08	1.6
	(0.2)	(0.3)	(0.7)	(0.03)	(1.1)	(0.01)	(0.4)
σ	0.47	0.51	0.26		0.19		
	(0.05)	(0.02)	(0.03)		(0.03)		
ρ	−0.70	−0.63	−0.81		−0.99		
	(0.07)	(0.03)	(0.08)		(0.13)		
ρ^{adj}		−0.52	−0.60		−0.69		
		(0.02)	(0.03)		(0.42)		

Table B.IV

Jump Parameters from Specific Models

This table presents the jump parameters of equation (B.1) above. The log futures jump sizes and annualized jump intensities for Poisson counter N_{jt} are

$$\gamma_j = \rho_J \gamma_{Vj} + \gamma_{fj} \sim (\bar{\gamma}_j, \delta_j^2),$$

$$\lambda_{jt} = \begin{cases} \lambda_{j1} V_{1t^*} & \text{for } j \leq 1 \\ \lambda_{j0} + \lambda_{j1} V_{1t^*} + \lambda_{jj} V_{jt^*} & \text{for } j > 1' \end{cases}$$

where $\gamma_{Vj} \sim \text{Exp}(\bar{\gamma}_{Vj})$ is the synchronous jump in annualized diffusive variance V_{jt}, γ_{fj} is an independent Gaussian shock, and V_{jt^*} is the variance at the start of the period. Log futures price jumps have correlation $\text{Corr}_j = \rho_j \bar{\gamma}_{Vj}/\delta_j$ with variance jumps, with no variance jumps ($\bar{\gamma}_{V0} = 0$) for Poisson counter N_{0t}. The γ_j parameters are in basis points; $\bar{\gamma}_1 = -0.051\%$ for the Vjump1a model, with a standard deviation of 0.326%. $\text{E}[\Delta N|J]$ is the expected number of additional jumps over a one-day or infinite horizon conditional on a variance jump of size $\bar{\gamma}_{Vj}$. Intradaily 15-minute periods were on average 1.20e-4 years, while the unconditional standard deviation of all 15-minute returns over 1983 to 2008 was 0.19%. Standard errors are in parentheses.

	Vjump1a	Vjump1b	
	N_{1t}	N_{0t}	N_{1t}
$\lambda_{j1} \times 10^{-4}$		38.3 (3.7)	
$\lambda_{jj} \times 10^{-4}$	2.0		0.31
	(0.1)		(0.02)
$\bar{\gamma}_j \times 10^4$	−5.1	−1.0	−20.4
	(0.7)	(0.1)	(4.0)
$\delta_j \times 10^4$	32.6	11.4	90.2
	(0.6)	(0.3)	(2.7)
$\bar{\gamma}_{Vj}$	0.0063		0.0115
	(0.0002)		(0.0006)
ρ_j	−0.27		−0.49
	(0.01)		(0.03)
Corr_j	−0.52		−0.62
	(0.02)		(0.03)
$\text{E}[\Delta N^{\text{day}}\|J]$	0.46	16.4	0.13
	(0.02)	(1.4)	(0.01)
$\text{E}[\Delta N^{\infty}\|J]$	2.63	131	1.05
	(0.16)	(14)	(0.09)

	Vjump2			Vjump3			
	N_{0t}	N_{1t}	N_{2t}	N_{0t}	N_{1t}	N_{2t}	N_{3t}
λ_{j0}			5.4			9.8	0.0
			(2.8)			(23.3)	(0.0)
$\lambda_{j1} \times 10^{-4}$	130		0.36	229		5.5	.09
	(30)		(0.06)	(82)		(1.3)	(.01)
$\lambda_{jj} \times 10^{-4}$		5.6	2.1		6.5	2.0	0.7
		(1.5)	(0.6)		(2.2)	(1.3)	(0.2)
$\bar{\gamma}_j \times 10^4$	−0.8	−2.3	−2.5	−0.6	0.2	−3.2	−19.9
	(0.2)	(1.4)	(3.9)	(0.2)	(1.7)	(2.2)	(8.6)

(*Continued*)

Table B.IV—*Continued*

	Vjump2			Vjump3			
	N_{0t}	N_{1t}	N_{2t}	N_{0t}	N_{1t}	N_{2t}	N_{3t}
$\delta_j \times 10^4$	6.9	20.2	36.5	5.6	17.8	6.3	103.3
	(0.5)	(1.6)	(2.5)	(0.5)	(1.6)	(6.4)	(7.1)
$\bar{\gamma}_{Vj}$		0.0016	0.070		0.0006	0.022	0.076
		(0.0002)	(0.011)		(0.0001)	(0.003)	(0.012)
ρ_j		−1.18	−0.05		−1.89	−0.02	−0.10
		(0.22)	(0.01)		(0.40)	(0.01)	(0.02)
Corr_j		−0.60	−0.92		−0.68	−0.83	−0.76
		(0.07)	(0.05)		(0.09)	(0.96)	(0.06)
$\text{E}[\Delta N^{\text{day}}\|J]$	5.1	0.22	2.6	5.6	0.16	0.20	1.7
	(1.1)	(0.04)	(0.3)	(1.6)	(0.03)	(0.11)	(0.2)
$\text{E}[\Delta N^{\infty}\|J]$	72	3.1	3.0	112	3.2	0.20	4.9
	(16)	(0.5)	(0.4)	(33)	(0.7)	(0.11)	(1.4)

Table B.V

Variance Factor Loadings

This table presents estimates of the individual and total contribution $V_{it}[1 + \sum_j \lambda_{ji}\text{E}(\gamma_j^2)]$ of each state variable V_{it} to diffusive and jump variances. Standard errors are in parentheses.

Model and V_i's	$E(V_{it})$	$SD(V_{it})$	Jump variance loading $\lambda_{ji}\text{E}(\gamma_j^2)$ on V_{it}				Total variance loading
			$j = 0$	1	2	3	
Vjump1a	0.0239	0.0211		0.22			1.22
V_1	(0.0008)	(0.0008)		(0.01)			(0.01)
Vjump1b	0.0171	0.0165	0.50	0.26			1.76
V_1	(0.0008)	(0.0010)	(0.03)	(0.02)			(0.04)
Vjump2							
V_1	0.0116	0.0077	0.63	0.23	0.05		1.91
	(0.0007)	(0.0005)	(0.07)	(0.03)	(0.01)		(0.09)
V_2	0.0066	0.0431			0.28		1.28
	(0.0007)	(0.0041)			(0.07)		(0.07)
Vjump3							
V_1	0.0085	0.0053	0.72	0.21	0.03	0.10	2.05
	(0.0008)	(0.0005)	(0.13)	(0.04)	(0.05)	(0.02)	(0.17)
V_2	0.0049	0.0118			0.01		1.01
	(0.0006)	(0.0009)			(0.02)		(0.02)
V_3	0.0051	0.0478				0.79	1.79
	(0.0013)	(0.0115)				(0.14)	(0.14)

Appendix C: Change of Measure

The pricing kernel specification affects three types of parameter values:

(i) the risk-neutral jump intensities and average jump sizes,
(ii) the risk-neutral rate of mean reversion of the jump-diffusive spot variance V_{1t}, and
(iii) the intraperiod conditional mean of futures returns.

For a pricing kernel with log changes of the form

$$d\ln\ \mathcal{M}_t = \mu_m\, dt + R\, d\ln F - \sum_i R_{Vi} dV_{it}, \tag{C.1}$$

the transformation from objective to risk-neutral jump intensities is

$$\begin{aligned}\frac{\lambda^*_{jt}}{\lambda_{jt}} &= \mathrm{E}\ \left[e^{d\ln \mathcal{M}_t} | dN_{jt} = 1\right] \\ &= \frac{\exp\left(-R\bar{\gamma}_{fj} + {}^1\!/_2 R^2 \delta^2_{fj}\right)}{1 - \left(R_{Vj} - R\rho_j\right)\bar{\gamma}_{Vj}}\ ,\end{aligned} \tag{C.2}$$

where $\gamma_{fj} \sim N(\bar{\gamma}_{fj},\ \delta^2_{fj})$ and $\gamma_{Vj} \sim \exp(\bar{\gamma}_{Vj})$ are the underlying Gaussian and exponential components of the j^{th} log futures jump $\gamma_j = \gamma_{fj} + \rho_j \gamma_{Vj}$.

The risk-neutral distribution for any jump $\tilde{\gamma}$ has a characteristic function

$$\mathrm{E}^*_t\ \left[e^{i\Phi\tilde{\gamma}}\right] = \frac{\mathrm{E}_t\left[e^{d\ln \mathcal{M}_t + e^{i\Phi\tilde{\gamma}}} | dN_t = 1\right]}{\mathrm{E}_t\left[e^{d\ln \mathcal{M}_t} | dN_t = 1\right]}\ . \tag{C.3}$$

The Gaussian shocks γ_{fj} remain Gaussian under this change of measure, with identical variance and shifted mean $\bar{\gamma}^*_{fj} = \bar{\gamma}_{fj} - R\delta^2_{fj}$. The exponential shocks γ_{Vj} remain exponential, with shifted mean

$$\bar{\gamma}^*_{Vj} = \frac{\bar{\gamma}_{Vj}}{1 - \left(R_{Vj} - R\rho_j\right)\bar{\gamma}_{Vj}}\ . \tag{C.4}$$

The overall mean jump in log futures prices becomes $\bar{\gamma}^*_j = \bar{\gamma}^*_{fj} + \rho_j \bar{\gamma}^*_{Vj}$, with associated expected percentage jump $\bar{k}^*_j = \exp(\bar{\gamma}^*_{fj} + {}^1\!/_2 \delta^2_{fj})/(1 - \rho_j\ \bar{\gamma}^*_{Vj}) - 1$.

The futures price is a martingale under the risk-neutral measure, with the log futures price evolving as

$$\begin{aligned} df_t &= \sum_{i=1}^{I}\left[-{}^1\!/_2 V_{it} dt + \sqrt{V_{it}} dW_{it}\right] + \sum_{j=1-K}^{J}\left(\gamma^*_j dN^*_{jt} - \lambda^*_{jt}\bar{k}^*_j dt\right), \\ dV_{1t} &= \left(\alpha - \beta^*_1 V_{1t}\right)\ dt + \sigma\sqrt{V_{1t}} dW^*_{Vt} + \gamma^*_{V1} dN^*_{1t}, \\ dV_{it} &= -\beta_i V_{it} dt + \gamma^*_{Vi} dN^*_{it}\ \text{ for }\ i > 1, \end{aligned} \tag{C.5}$$

Table C.I

Objective versus Risk-Neutral Parameters from Vjump3 Estimates

This table presents estimates of the change of measure from objective to risk-neutral parameters for the Vjump3 model, based on constrained and unconstrained values of the risk aversion parameters $(R;\ \boldsymbol{R}_V)$ that best fit option prices. The rp1 parameters are from Bates (2012). The rp2 parameters are constrained to be positive, while the rp3 parameters are unconstrained.

rp1 : $(R;\ \boldsymbol{R}_V) = (2.45; \mathbf{0})$; $(\beta_1, \beta_1^*) = (54.59, 54.14)$;
rp2 : $(R;\ \boldsymbol{R}_V) = (0.075; .001, 10.37, .074)$; $(\beta_1, \beta_1^*) = (54.59, 54.58)$;
rp3 : $(R;\ \boldsymbol{R}_V) = (300; -933, 2.17, -34.6)$; $(\beta_1, \beta_1^*) = (54.59, 31.42)$.

	Jump j			
Jump Parameters	0	1	2	3
$\lambda_{jt}^*/\lambda_{jt}$ |rp1	1.0002	0.9996	1.0008	1.0052
$\lambda_{jt}^*/\lambda_{jt}$ |rp2	1.0000	1.0000	1.2916	1.0058
$\lambda_{jt}^*/\lambda_{jt}$ |rp3	1.0328	0.6066	1.1877	1.0640
$\bar{\gamma}_{Vj}$		0.000637	0.0218	0.0758
$\bar{\gamma}_{Vj}^*$ |rp1		0.000638	0.0218	0.0772
$\bar{\gamma}_{Vj}^*$ |rp2		0.000637	0.0281	0.0762
$\bar{\gamma}_{Vj}^*$ |rp3		0.000516	0.0273	0.0591
$\bar{k}_j$	−0.00608%	0.00230%	−0.0317%	−0.194%
$\bar{k}_j^*$ |rp1	−0.00616%	0.00153%	−0.0318%	−0.220%
$\bar{k}_j^*$ |rp2	−0.00609%	0.00228%	−0.0469%	−0.199%
$\bar{k}_j^*$ |rp3	−0.01538%	−0.02627%	−0.0487%	−1.384%

where $\beta_1^* = \beta_1 + R\rho\sigma - R_{V1}\sigma^2$ and N_{jt}^* are Poisson counters with intensity $\lambda_{jt}^* = \lambda_{jt}\left(\frac{\lambda_{jt}^*}{\lambda_{jt}}\right)$.

The instantaneous expected percentage return of the futures price under the objective measure is the conditional equity premium, which takes the form

$$\left(\mu_{0t} + \sum_i \mu_i V_{it}\right) dt = -\mathrm{E}_t\left[\left(\frac{dF_t}{F_t}\right)\left(\frac{d\mathcal{M}_t}{\mathcal{M}_t}\right)\right]. \tag{C.6}$$

Because jump intensities are assumed constant within periods, with a linear dependency on the spot variances at the start of the period, the intraperiod parameter values are

$$\begin{aligned} \mu_{0t} &= \sum_j \lambda_{jt}\left(\bar{k}_j - \frac{\lambda_{jt}^*}{\lambda_{jt}}\bar{k}_j^*\right), \\ \mu_1 &= R - R_{V1}\rho\sigma, \\ \mu_i &= R \text{ for } i > 1, \end{aligned} \tag{C.7}$$

where λ_{jt} is specified in equation (3) and the ratio $\lambda_{jt}^*/\lambda_{jt}$ is a constant given in (C.2).

REFERENCES

Abramowitz, Milton, and Irene A. Stegun, 1972, *Handbook of Mathematical Functions* (Dover, New York).

Aït-Sahalia, Yacine, Julio Cacho-Diaz, and Roger J.A. Laeven, 2015, Modeling financial contagion using mutually exciting jump processes, *Journal of Financial Economics* 117, 585–606.

Aït-Sahalia, Yacine, and Jean Jacod, 2014, *High-Frequency Financial Economics* (Princeton University Press, Princeton, NJ).

Andersen, Torben G., 2004, Discussion [of Barndorff-Nielsen and Shephard (2004)], *Journal of Financial Econometrics* 2, 37–48.

Andersen, Torben G., and Tim Bollerslev, 1997. Intraday periodicity and volatility persistence in financial markets, *Journal of Empirical Finance* 4, 115–158.

Andersen, Torben G., and Tim Bollerslev, 1998, Deutsche mark-dollar volatility: Intraday activity patterns, macroeconomic announcements, and longer run dependencies, *Journal of Finance* 53, 219–265.

Andersen, Torben G., Nicola Fusari, and Victor Todorov, 2015, The risk premia embedded in index options, *Journal of Financial Economics* 117, 558–584.

Andersen, Torben G., Nicola Fusari, and Victor Todorov, 2017, Short-term market risks implied by weekly options, *Journal of Finance* 72, 1335–1386.

Backus, David K., Silverio Foresi, Kai Li, and Liuren Wu, 1997, Accounting for biases in Black Scholes, Working paper, New York University.

Bakshi, Gurdip, Nikunj Kapadia, and Dilip B. Madan, 2003, Stock return characteristics, skew laws, and the differential pricing of individual equity options, *Review of Financial Studies* 16, 1–101.

Bandi, Federico M., and Roberto Renò, 2016, Price and volatility co-jumps, *Journal of Financial Economics* 119, 107–146.

Barndorff-Nielsen, Ole E., and Neil Shephard, 2004, Power and bipower variation with stochastic volatility and jumps, *Journal of Financial Econometrics* 2, 1–37.

Barndorff-Nielsen, Ole E., and Neil Shephard, 2006, Econometrics of testing for jumps in financial economics using bipower variation, *Journal of Financial Econometrics* 4, 1–30.

Bates, David S., 1991, The crash of '87: Was it expected? The evidence from options markets, *Journal of Finance* 46, 1009–1044.

Bates, David S., 1996, Jumps and stochastic volatility: Exchange rate processes implicit in deutsche mark options, *Review of Financial Studies* 9, 69–107.

Bates, David S., 1997, The skewness premium: Option pricing under asymmetric processes, *Advances in Futures and Options Research* 9, 51–82.

Bates, David S., 2000, Post-'87 crash fears in the S&P 500 futures option market, *Journal of Econometrics* 94, 181–238.

Bates, David S., 2006, Maximum likelihood estimation of latent affine processes, *Review of Financial Studies* 19, 909–965.

Bates, David S., 2012, U.S. stock market crash risk, 1926–2010, *Journal of Financial Economics* 105, 229–259.

Black, Fischer, 1976, The pricing of commodity contracts, *Journal of Financial Economics* 3, 167–179.

Broadie, Mark N., Mikhail Chernov, and Michael Johannes, 2007, Model specification and risk premiums: Evidence from futures options, *Journal of Finance* 62, 1453–1490.

Calvet, Laurent, and Adlai J. Fisher, 2008, *Multifractal Volatility: Theory, Forecasting, and Pricing* (Academic Press, Amsterdam).

Campbell, John Y., Andrew W. Lo, and A. Craig MacKinlay, 1997. *The Econometrics of Financial Markets* (Princeton University Press, Princeton, NJ).

Carlson, Mark, 2006, A brief history of the 1987 stock market crash with a discussion of the Federal Reserve response, Working paper, Board of Governors of the Federal Reserve.

Carr, Peter, and Liuren Wu, 2008, Leverage effect, volatility feedback, and self-exciting market disruptions: Disentangling the multi-dimensional variations in S&P 500 index options, Working paper, Baruch College.

Chan, Kalok, Ceajer K. Chan, and G. Andrew Karolyi, 1991, Intraday volatility in the stock index and stock index futures market, *Review of Financial Studies* 4, 657–684.

Chernov, Mikhail, A. Ronald Gallant, Eric Ghysels, and George Tauchen, 2003, Alternative models for stock price dynamics, *Journal of Econometrics* 116, 225–257.

Das, Sanjiv R., and Rangarajan K. Sundaram, 1999, Of smiles and smirks: A term-structure perspective, *Journal of Financial and Quantitative Analysis* 34, 211–239.

Duffie, Darrell, Jun Pan, and Kenneth J. Singleton, 2000, Transform analysis and asset pricing for affine jump-diffusions, *Econometrica* 68, 1343–1376.

Eraker, Bjorn, Michael Johannes, and Nicholas G. Polson, 2003, The impact of jumps in volatility and returns, *Journal of Finance* 58, 1269–300.

Fulop, Andras, Junye Li, and Jun Yu, 2015, Self-exciting jumps, learning, and asset pricing implications, *Review of Financial Studies* 28, 876–912.

Gallant, A. Ronald, 1981, On the bias in flexible functional forms and an essentially unbiased form: The Fourier flexible form, *Journal of Econometrics* 15, 211–245.

Hausman, Jerry A., Andrew W. Lo, and A. Craig MacKinlay, 1992, An ordered probit analysis of transaction stock prices, *Journal of Financial Economics* 31, 319–379.

Heston, Steve L., 1993, A closed-form solution for options with stochastic volatility with applications to bond and currency options, *Review of Financial Studies* 6, 327–344.

Jacod, Jean, and Victor Todorov, 2010, Do price and volatility jump together? *Annals of Applied Probability* 20, 1425–1469.

Jones, Christopher S., 2003, The dynamics of stochastic volatility: Evidence from underlying and options markets, *Journal of Econometrics* 116, 147–180.

Lee, Suzanne S., and Per A. Mykland, 2008, Jumps in financial markets: A new nonparametric test and jump dynamics, *Review of Financial Studies* 21, 2535–2563.

Mancini, Cecilia, 2009, Nonparametric threshold estimation for models with stochastic diffusion coefficient and jumps, *Scandinavian Journal of Statistics* 36, 270–296.

Merton, Robert C., 1976. Option pricing when underlying stock returns are discontinuous, *Journal of Financial Economics* 3, 125–144.

Poppe, Gert P.M., and Christianus M.J. Wijers, 1990, More efficient computation of the complex error function, *ACM Transactions on Mathematical Software* 16, 38–46.

Prokopczuk, Marcel, and Chardin Wese Simen, 2014, What makes the market jump? Working paper, Leibniz University Hannover.

Stroud, Jonathan R., and Michael Johannes, 2014, Bayesian modeling and forecasting of 24-hour high-frequency volatility, *Journal of the American Statistical Association* 109, 1368–1384.

Tauchen, George, and Hao Zhou, 2011, Realized jumps on financial markets and predicting credit spreads, *Journal of Econometrics* 160, 102–118.